Journal of Applied Analysis and Computation
Volume 17, Number 1, February 2027, 212–254
Website:http://www.jaac-online.com
DOI:10.11948/20260014

# BIFURCATIONS AND EXACT TRAVELING WAVE SOLUTIONS FOR A GENERALIZED KLEIN- GORDON EQUATION WITH BETA FRACTIONAL DERIVATIVES

**Nail Turhan[1,2,†], Ali Deliceoğlu[2] and Yusuf Pandır[3]**

**Abstract** In this paper, we consider the exact traveling wave solutions of the generalized Klein-Gordon equation with beta fractional derivatives. By using the bifurcation theory of dynamical systems, we derive the bifurcation behavior of its phase portraits under various parameter settings. For some special level curves, we obtain all possible traveling wave solutions such as periodic wave solutions, dark and bright solitary wave solutions, kink and anti-kink solutions, and some unbounded wave solutions. The impacts of beta fractional orders are analyzed using graphs, with a focus on their impact on temporal delay, broadening, and the oscillation period. Furthermore, the present work generalizes and extends earlier findings in the literature. These results contribute to a deeper understanding of the dynamics of the generalized Klein-Gordon equation model with beta fractional derivatives.

**Keywords** Bifurcation, Klein-Gordon equation, traveling wave solution, singular dynamical systems, beta fractional derivative.

**MSC(2010)** 35C07, 34C23, 34A08, 35Q51, 34C37.

## 1. Introduction

Nonlinear partial differential equations can represent several nonlinear phenomena in disciplines such as hydrodynamics, fluid dynamics, optics, and applied mathematics. Research on nonlinear partial differential equations is crucial for explaining the evolution of nonlinear dynamics. The Klein-Gordon (KG) equation plays a key role in quantum physics, especially within the framework of relativistic quantum mechanics. This equation can also be used to characterize dispersive wave events in relativistic frameworks. Furthermore, the KG equation is widely used in areas such as nonlinear optical phenomena and plasma physics, occurring in both linear and nonlinear versions [24]. The derivation of soliton and periodic wave solutions by Jacobi elliptic functions has been investigated for nonlinear Klein–Gordon-type equations, wherein both topological and non-topological structures arise based on the nonlinearity [12, 13].

Traveling waves have become an essential subject in recent research due to their complex structure and applications in various physical models. The analytical and nonanalytical traveling wave behaviors of the (n+1)-dimensional Klein–Gordon equation were investigated in [12] using bifurcation theory. They obtained analytic and nonanalytic traveling wave solutions, including solitary, periodic, and cusp-type waves. In 2023, Arab [3] used the qualitative theory of

†The corresponding author.
[1]Graduate School of Natural and Applied Sciences, Erciyes University, Kayseri 38039, Turkey
[2]Department of Mathematics, Erciyes University, Kayseri 38039, Turkey
[3]Department of Mathematics, Yozgat Bozok University, Yozgat 66100, Turkey
Email: nxturhan@gmail.com(N. Turhan), adelice@erciyes.edu.tr(A. Deliceoğlu),
yusufpandir@gmail.com(Y. Pandır)

planar dynamical systems to construct traveling wave solutions—including periodic, kink (anti-kink), and solitary waves for the nonlinear Klein–Gordon equation. By reducing the equation to a one-dimensional Hamiltonian system, the authors analyzed phase portraits and obtained various exact solutions through bifurcation analysis. Some of the studies conducted on the Klein–Gordon equation using the bifurcation method and the qualitative theory of dynamical systems are as follows: The singular soliton solutions of the second-order nonlinear Klein–Gordon equation have been expressed as traveling wave solutions using the Ansatz approach [27]. The localized traveling-wave (solitary) solutions of the Klein–Gordon equation with cubic nonlinearity, including bell-shaped solitary waves, kink-shaped solitary waves, and periodic solutions expressed in terms of Jacobi elliptic functions, have been obtained [30]. By investigating the traveling wave solutions of generalized nonlinear Klein–Gordon model equations, the effects of horizontal singular lines and the corresponding singular solutions have been presented [33]. Within the framework of the Klein–Gordon system, exact solutions describing the propagation of compact waves and motions with oscillatory spatial dependence have been obtained [34].

Several fractional derivatives have been established in the field of fractional calculus. The most frequently used fractional derivatives include Caputo, Liouville, and conformable derivatives (see, for example, [8, 18, 25]). The beta-derivative, introduced by Atangana et al. in [6], generalizes the classical derivative while addressing limitations inherent in fractional calculus. The dynamical behavior of the Sakovich equation with beta derivatives was examined using the qualitative theory of planar dynamical systems, resulting in periodic, solitary, and kink solutions [2]. Additionally, exact and semi-analytic solutions were obtained by applying the modified extended tanh function method and the homotopy analysis method to the Klein-Fock-Gordon equation with a beta derivative [29]. Optical soliton solutions were investigated for the fractional-order nonlinear Schrödinger equation with a parabolic law by using the generalized auxiliary equation method and the $(\frac{1}{G'})$-expansion method [4]. Exact analytical solutions, soliton, and periodic wave solutions have been obtained in the time-fractional Gardner equation using the improved F-expansion approach [16]. Recently, various exact soliton and traveling wave solutions together with graphical representations have been reported for different forms of fractional Klein–Gordon and other nonlinear fractional evolution equations by using methods such as the extended fractional Riccati expansion method, fractal functional variable method, fractal sech-function method, and several direct analytical approaches [7, 23, 26, 28].

Studies involving the nonlinear Klein-Gordon (KG) equation with fractional derivatives have been conducted using the conformable derivative [14] and focusing on bifurcation behavior [10]. By using the Riemann-Liouville fractional derivative, perturbation analysis was performed to obtain the analytical periodic solutions of the KG equation [11]. A comprehensive examination of exact solutions has been carried out by applying the combined method and the modified Khater method within the Phi-4 equation, which has a fractional derivative in the KG equation model [1].

In 2014, Mirzazadeh et al. [24] studied the following two variants of the nonlinear Klein–Gordon (GKG) equations:

$$(q^m)_{tt} - k^2(q^m)_{xx} + a\, q^m - b\, q^{m-n} + c\, q^{n+m} = 0, \tag{1.1}$$

$$(q^m)_{tt} - k^2(q^m)_{xx} + a\, q^m - b\, q^n + c\, q^{2n-m} = 0, \tag{1.2}$$

where q = q(x, t) represents the wave form of the unknown function; $a$, $b$, $c$, and $k$ are real-valued constants; $m \in \mathbb{Z}$ with $m \geq 1$, and $n$ is a nonlinear parameter. The authors successfully applied the $\left(\frac{G'}{G}\right)$-expansion method to obtain exact solitary wave solutions for two different forms of the Klein–Gordon equations with full nonlinearity, demonstrating the method's efficiency and broad applicability in solving nonlinear evolution equations in mathematical physics. Inspired by this approach, we aim to explore an alternative nonlinear model and analyze the resulting wave dynamics under beta fractional derivative.

In this study, we extend the generalized Klein-Gordon (GKG) equations considered in [24] by modifying the GKG equation to include beta fractional derivatives, and perform a bifurcation analysis to investigate the resulting wave dynamics. Due to the strong nonlinearity of the generalized Eqs. (1.1) and (1.2), obtaining closed-form solutions is highly challenging. Therefore, we apply the bifurcation theory of planar dynamical systems [12] to qualitatively analyze the traveling wave behavior, constructing explicit solutions in terms of trigonometric, rational, Jacobi elliptic and hyperbolic functions through the analysis of phase portraits.

The present study contributes to the literature in several aspects. First, the generalized Klein–Gordon equation is extended to the beta-derivative framework within the context of bifurcation theory and singular dynamical systems. Second, several exact traveling wave solutions are derived, including periodic, solitary, kink, anti-kink, and singular wave solutions. Furthermore, the influence of the beta fractional orders on the wave structures is illustrated graphically. Compared with existing studies on classical and fractional Klein–Gordon equations, the present work provides a qualitative bifurcation analysis together with explicit traveling wave solutions obtained from phase portrait analysis, thereby enriching the current literature.

The rest of the paper is organized as follows. In Sect. 2, the definition and fundamental properties of the beta-derivative are presented, and the generalized KG equation is reformulated using the beta-derivative. In Sect. 3, the bifurcation behavior and exact traveling wave solutions of Eq. (1.1) are examined, while Sect. 4 focuses on the same analysis for Eq. (1.2). In Sect. 5, several exact traveling wave solutions are illustrated using $3D$, contour, and $2D$ plots to investigate the influence of the beta derivative on the wave profiles. Finally, Sect. 6 summarizes the findings of this work.

## 2. Definition and some features about the beta-derivative

In this section, properties of $\beta$ derivative are given.

**Definition 2.1.** [5] Let $\psi$ be a function defined for all nonnegative $t$. Then, the beta derivative of $\psi$ of order $\beta$ is given by

$$\frac{\partial^\beta \psi(t)}{\partial t^\beta} = \lim_{\delta\to 0} \frac{\psi(t+\delta(t+\frac{1}{\Gamma(\beta)})^{1-\beta}) - \psi(t)}{\delta}, \quad \delta > 0, \quad 0 < \beta \leq 1. \tag{2.1}$$

Some useful properties of the beta derivative are presented in [5].

**Theorem 2.1.** *Let $\psi(t)$ and $\phi(t)$ be $\beta$-differentiable functions for all $t > 0$ and $\beta \in (0, 1]$. Then*

*(i)* $\frac{\partial^\beta}{\partial t^\beta}(\psi(t)) = \left(t + \frac{1}{\Gamma(\beta)}\right)^{1-\beta} \frac{d\psi(t)}{dt} = \left(t + \frac{1}{\Gamma(\beta)}\right)^{1-\beta} \psi'(t).$

*(ii)* $\frac{\partial^\beta}{\partial t^\beta}(c) = 0, \quad c \in \mathbb{R}.$

*(iii)* $\frac{\partial^\beta}{\partial t^\beta}\{a\psi(t) + b\phi(t)\} = a\frac{\partial^\beta}{\partial t^\beta}(\psi(t)) + b\frac{\partial^\beta}{\partial t^\beta}(\phi(t)), \quad \forall\, a, b \in \mathbb{R}.$

*(iv)* $\frac{\partial^\beta}{\partial t^\beta}\{\psi(\phi(t))\} = \left(t + \frac{1}{\Gamma(\beta)}\right)^{1-\beta} \psi'(\phi(t))\, \phi'(t).$

*(v)* $\frac{\partial^{\beta}}{\partial t^{\beta}}\left\{\psi\left(t\right)\phi\left(t\right)\right\}=\frac{\partial^{\beta}}{\partial t^{\beta}}\left(\psi\left(t\right)\right)\phi\left(t\right)+\frac{\partial^{\beta}}{\partial t^{\beta}}\left(\phi\left(t\right)\right)\psi\left(t\right).$

*(vi)* $\frac{\partial^{\beta}}{\partial t^{\beta}}\left\{\frac{\psi(t)}{\phi(t)}\right\}=\frac{\frac{\partial^{\beta}}{\partial t^{\beta}}(\psi(t))\phi(t)-\frac{\partial^{\beta}}{\partial t^{\beta}}(\phi(t))\psi(t)}{[\phi(t)]^2}.$

### 2.1. Beta-derivative governing equation

In this section, the GKG equation is expressed according to the $\beta$-derivative operator. It preserves several useful properties of the classical derivative, which makes the traveling wave reduction and bifurcation analysis applicable.

The reduced ordinary differential equation can be obtained using wave transform to Eqs. (1.1) and (1.2). The $\beta$-derivative version of Eqs. (1.1) and (1.2) are given by

$$\frac{\partial^{2\beta_1}}{\partial t^{2\beta_1}}(q^m)-k^2\frac{\partial^{2\beta_2}}{\partial x^{2\beta_2}}(q^m)+a\ q^m-b\ q^{m-n}+c\ q^{n+m}=0, \tag{2.2}$$

$$\frac{\partial^{2\beta_1}}{\partial t^{2\beta_1}}(q^m)-k^2\frac{\partial^{2\beta_2}}{\partial x^{2\beta_2}}(q^m)+a\ q^m-b\ q^{n}+c\ q^{2n-m}=0, \tag{2.3}$$

where $0<\beta_i<1 (i=1,2)$, and $\frac{\partial^{2\beta}}{\partial t^{2\beta}}$, $\frac{\partial^{2\beta}}{\partial x^{2\beta}}$ represents the $\beta$-derivative with respect to time and space, respectively. We use bifurcation methods to study the behavior of solutions in fractional and classical differential equations [9,17,19–22,31,32,35,36] to investigate the dynamical behavior of Eqs. (2.2) and (2.3). To the best of our knowledge, the $\beta$-derivative GKG equation has not been previously studied. Here, we present some of its wave solutions and discuss the effect of the derivative order [2].

To obtain all possible exact solutions of the GKG equation with the beta derivative, we consider the following wave variable transformation:

$$q=q(x,t)=\psi(\xi),\qquad \xi=\lambda\left(t+\frac{1}{\Gamma(\beta_1)}\right)^{\beta_1}+\alpha\left(x+\frac{1}{\Gamma(\beta_2)}\right)^{\beta_2}, \tag{2.4}$$

where $\lambda$ is the wave speed, $\alpha$ represents the wave parameter, and $\Gamma(\cdot)$ is the Gamma function. This transformation allows the fractional partial differential equations to be reduced to ordinary differential equations.

Using the properties of the $\beta$-derivative together with the traveling wave transformation, we obtain

$$\frac{\partial^{2\beta_1}}{\partial t^{2\beta_1}}(q^m)=\lambda^2\beta_1^2(\psi^m)'',\qquad \frac{\partial^{2\beta_2}}{\partial x^{2\beta_2}}(q^m)=\alpha^2\beta_2^2(\psi^m)''.$$

Substituting these relations into Eq. (2.2), we get

$$p(\psi^m)''+a\psi^m-b\psi^{m-n}+c\psi^{m+n}=0,$$

where $p=\lambda^2\beta_1^2-k^2\alpha^2\beta_2^2$. Using the identity

$$(\psi^m)''=m(m-1)\psi^{m-2}(\psi')^2+m\psi^{m-1}\psi'',$$

and multiplying the resulting equation by $\psi^{2-m}$, we obtain

$$m(m-1)p(\psi')^2+mp\psi\psi''+a\psi^2-b\psi^{2-n}+c\psi^{n+2}=0. \tag{2.5}$$

Similarly, applying the same procedure to Eq. (2.3), we obtain

$$m(m-1)p(\psi')^2+mp\psi\psi''+a\psi^2-b\psi^{n-m+2}+c\psi^{2n-2m+2}=0. \tag{2.6}$$

# 3. Bifurcations of phase portraits of Eq. (2.5)

In this section, we consider the phase portraits of Eq. (2.5). First, applying the transformation

$$\psi = v^{\frac{1}{n}},$$

to Eq. (2.5), we obtain

$$\psi'' = \frac{1}{n}\left(\frac{1}{n}-1\right) v^{\frac{1}{n}-2}(v')^2 + \frac{1}{n} v^{\frac{1}{n}-1} v''.$$

Substituting this expression into Eq. (2.5) gives

$$\frac{mp(m-n)}{n^2} v^{\frac{2}{n}-2}(v')^2 + \frac{mp}{n} v^{\frac{2}{n}-1} v'' + a v^{\frac{2}{n}} - b v^{\frac{2}{n}-1} + c v^{\frac{2}{n}+1} = 0.$$

Multiplying this equation by $v^{2-\frac{2}{n}}$, we obtain

$$\frac{mp(m-n)}{n^2}(v')^2 + \frac{mp}{n} v v'' - bv + av^2 + cv^3 = 0. \tag{3.1}$$

Eq. (3.1) is equivalent to the two-dimensional system as follows:

$$\frac{dv}{d\xi} = y, \quad \frac{dy}{d\xi} = \frac{-\frac{mp(m-n)}{n^2} y^2 + bv - av^2 - cv^3}{\frac{mp}{n} v}. \tag{3.2}$$

To study the exact explicit solutions of Eq. (3.1), we need to investigate the dynamical behaviour of the system (3.2) depending on the six parameter group $(n, m, p, a, b, c)$. System (3.2) has the following first integral:

$$H(v, y) = v^{\frac{2m}{n}-2}\left(\frac{mp}{2n} y^2 - \frac{bn}{2m-n} v + \frac{an}{2m} v^2 + \frac{cn}{2m+n} v^3\right) = h, \tag{3.3}$$

where h is an arbitrary constant. Eq. (3.3) yields the wave-type solutions to be derived from the phase portraits in the subsequent sections. Furthermore, the existence of a solution to the singular system requires that $m \neq n$. When $m = n$, the system admits solutions that do not involve singularities. From Eq. (3.3), we derive the necessary conditions on the parameters $m$ and $n$ under which explicit solutions can be obtained.

We consider the regular systems associated with system (3.2) as follows:

$$\frac{dv}{d\zeta} = \frac{mp}{n} yv, \qquad \frac{dy}{d\zeta} = -\frac{mp(m-n)}{n^2} y^2 + bv - av^2 - cv^3. \tag{3.4}$$

This system has the same level curves as (3.2), where $d\xi = \frac{mp}{n} v\, d\zeta$. To analyze the phase portrait of this system, it is crucial to first determine the equilibrium points by setting the derivatives $\frac{dv}{d\zeta} = 0$ and $\frac{dy}{d\zeta} = 0$ [15]. By solving these equations, we can obtain at most three equilibrium points: $E_0(v_0, 0)$, $E_1(v_1, 0)$ and $E_2(v_2, 0)$, where $v_0 = 0$, $v_1 = \frac{-a-\sqrt{a^2+4bc}}{2c}$ and $v_2 = \frac{-a+\sqrt{a^2+4bc}}{2c}$.

Assume the equilibrium point of system (3.4) is $E_i(v_i, 0)$ $(i = 0, 1, 2)$, then the corresponding Jacobi matrix is

$$M(v_i, 0) = \begin{bmatrix} 0 & \frac{mp}{n} v_i \\ b - 2av_i - 3c{v_i}^2 & 0 \end{bmatrix},$$

from the above, we get

$$det(M(v_i,0)) = J(v_i,0) = \frac{mp}{n} v_i \left(3c{v_i}^2 + 2av_i - b\right).$$

This determinant can also be written in terms of the components of the equilibrium points as follows:

$$J(v_i,0) = \frac{cmp}{n} v_i[(v_i - v_1)(v_i - v_2) + v_i(v_i - v_2) + v_i(v_i - v_1)]. \tag{3.5}$$

According to (3.5), we have $J(0,0) = 0$, $J(v_1,0) = \frac{3cmp}{n} v_1^2(v_1 - v_2)$ and $J(v_2,0) = \frac{3cmp}{n} v_2^2(v_2 - v_1)$. By the theory of planar dynamical systems, for an equilibrium point of a planar integrable system, if $J < 0$, then the equilibrium point is a saddle point; if $J > 0$, then it is a center point; if $J = 0$ and the Poincaré index of the equilibrium point is 0, then this equilibrium point is a cusp.

To obtain the explicit parametric representations of the traveling wave solutions of Eq. (2.2), we discuss the following five cases and obtain the corresponding phase portraits of the system (3.4) shown in Figures 1-4.

1. We assume that $\Delta = a^2 + 4bc > 0$, $p > 0$, and $n < 0$. It is easy to see that the distribution of the equilibrium points of (3.4) is as follows:
   (a) For $c > 0$, we have
      i. If $a \neq 0$ and $b > 0$, then $v_1 < 0 < v_2$, in which case the equilibrium point $E_1(v_1,0)$ is a center, and $E_2(v_2,0)$ is a saddle (see Figure 1a).
      ii. If $a > 0$ and $b < 0$, then $v_1 < v_2 < 0$, and the equilibrium points satisfy: $E_1(v_1,0)$ is a center, $E_2(v_2,0)$ is a saddle (see Figure 1b).
      iii. If $a < 0$ and $b < 0$, then $0 < v_1 < v_2$, in which case $E_1(v_1,0)$ is a center, and $E_2(v_2,0)$ is a saddle (see Figure 1c).

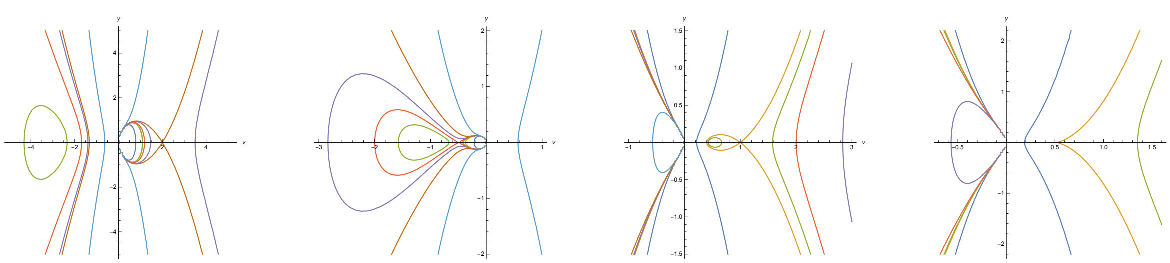

(a) $a > 0,\ b > 0,\ \Delta > 0$ (b) $a > 0,\ b < 0,\ \Delta > 0$ (c) $a < 0,\ b < 0,\ \Delta > 0$ (d) $a < 0,\ b < 0,\ \Delta = 0$

**Figure 1.** The phase portraits of system (3.4) for $c > 0$, $p > 0$, and $n < 0$.

   (b) For $c < 0$, we have
      i. If $a > 0$ and $b > 0$, then $0 < v_2 < v_1$, in which case $E_1(v_1,0)$ is a center, and $E_2(v_2,0)$ is a saddle (see Figure 2a).
      ii. If $a < 0$ and $b > 0$, then $v_2 < v_1 < 0$, and similarly, $E_1(v_1,0)$ is a center, while $E_2(v_2,0)$ is a saddle (see Figure 2b).
      iii. If $a \neq 0$ and $b < 0$, then $v_2 < 0 < v_1$; in this case, $E_1(v_1,0)$ is a center, and $E_2(v_2,0)$ is a saddle (see Figure 2c).

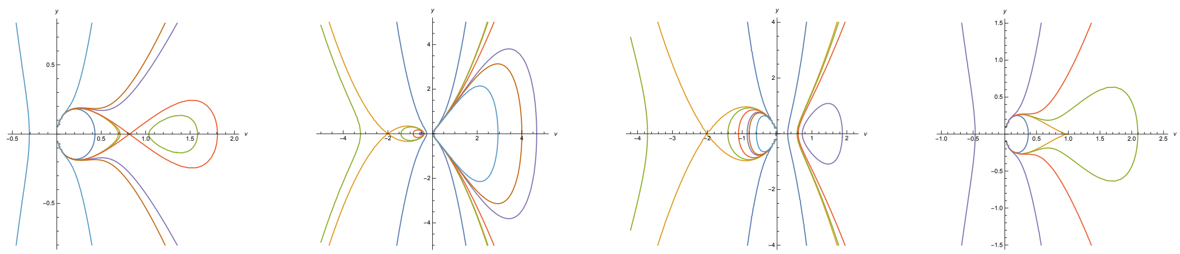

(a) $a > 0$, $b > 0$, $\Delta > 0$ (b) $a < 0$, $b > 0$, $\Delta > 0$ (c) $a < 0$, $b < 0$, $\Delta > 0$ (d) $a > 0$, $b > 0$, $\Delta = 0$

**Figure 2.** The phase portraits of system (3.4) for $c < 0$, $p > 0$, and $n < 0$.

2. When $\Delta = a^2 + 4bc = 0$, system (3.4) has a double root at $v_1 = v_2 = -\frac{a}{2c}$. In this case, the Jacobian evaluated at the equilibrium points $E_0(0, 0)$ and $E_1(v_1, 0)$ satisfies $J(v_i, 0) = 0$, indicating that both equilibrium points are cusp-type singularities (see Figures 1d and 2d).
3. We assume that $b = 0$, $p > 0$, and $n > 0$. In this case, system (3.4) has two equilibrium points $E_0(0, 0)$, $E_1(v_1, 0)$, where $v_1 = -\frac{a}{c}$. At each equilibrium point $E_i(v_i, 0)$, the determinant of the Jacobian matrix is given by $J(v_i, 0) = \frac{mp}{n} {v_i}^2 (3cv_i + 2a)$. In particular, $J(0, 0) = 0$, $J(v_1, 0) = -\frac{mpa^3}{nc^2}$. This case is analyzed within the framework of bifurcation theory. For $c \neq 0$, we have
   (a) If $a > 0$, then the equilibrium point $E_1(v_1, 0)$ is a saddle (see Figures 3a and 3c).
   (b) If $a < 0$, then the equilibrium point $E_1(v_1, 0)$ is a center (see Figures 3b and 3d).

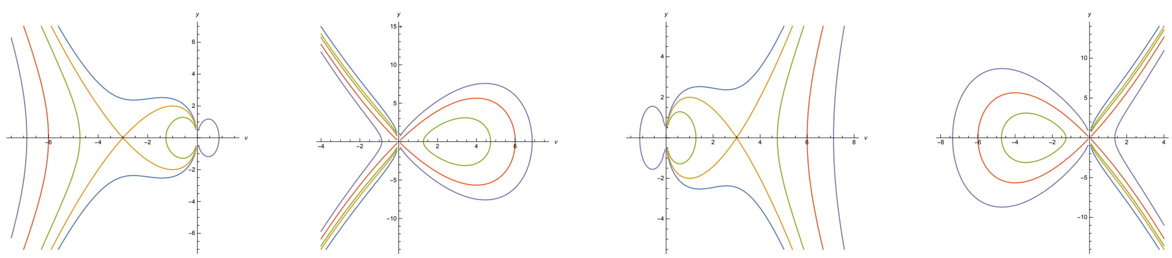

(a) $a > 0$, $c > 0$ (b) $a < 0$, $c > 0$ (c) $a > 0$, $c < 0$ (d) $a < 0$, $c < 0$

**Figure 3.** The phase portraits of system (3.4) for $b = 0$, $p > 0$, and $n > 0$.

4. We assume that $c = 0$, $p > 0$, and $n > 0$. In this case, system (3.4) has two equilibrium points, $E_0(0, 0)$, $E_1(v_1, 0)$, where $v_1 = b/a$. At the equilibrium point $E_i(v_i, 0)$, the determinant of the Jacobian matrix is given by $J(v_i, 0) = \frac{mp}{n} v_i (2av_i - b)$. This yields $J(0, 0) = 0$, $J(v_1, 0) = \frac{mpb^2}{na}$. This case is analyzed within the context of bifurcation theory. For $b \neq 0$, we have
   (a) If $a > 0$, then $E_1(v_1, 0)$ is a saddle (see Figures 4a and 4b).
   (b) If $a < 0$, then $E_1(v_1, 0)$ is a center (see Figures 4c and 4d).

**Remark 3.1.** When $p < 0$, the stability of the equilibrium points previously analyzed is reversed: Saddles become centers, and centers become saddles. In this case, the phase portraits corresponding to $p < 0$ are symmetric counterparts of the original ones associated with $p > 0$.

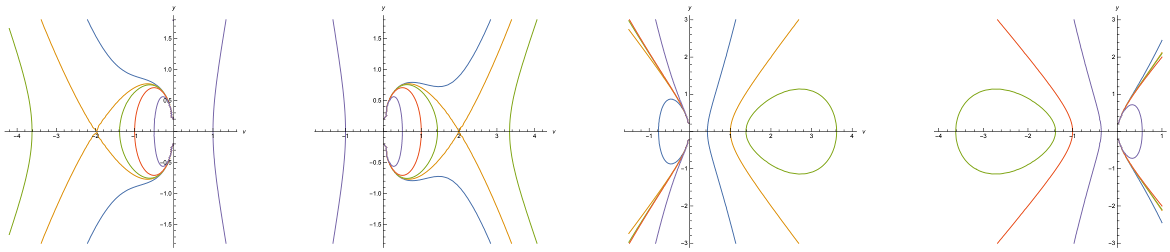

(a) $a > 0$, $b < 0$ (b) $a > 0$, $b > 0$ (c) $a < 0$, $b < 0$ (d) $a < 0$, $b > 0$

**Figure 4.** The phase portraits of system (3.4) for $c = 0$, $p > 0$, $n < 0$.

### 3.1. The exact traveling wave solutions of Eq. (2.5) given by the level curves $H(v, y) = 0$

In this section, we obtain the possible exact explicit parametric solutions of Eq. (2.2) for different parametric conditions. When $h = 0$, Eq. (3.3) yields that

$$y^2 = \frac{2n^2}{mp}\left(\frac{b}{2m-n}v - \frac{a}{2m}v^2 - \frac{c}{2m+n}v^3\right). \tag{3.6}$$

By integrating the first equation of system (3.2), we obtain

$$\int_{v_j}^{v} \frac{dv}{\sqrt{v\left(\frac{b}{2m-n} - \frac{a}{2m}v - \frac{c}{2m+n}v^2\right)}} = \pm\sqrt{\frac{2n^2}{m|p|}}(\xi - \xi_0), \tag{3.7}$$

where $v = v(\xi)$ is the solution of Eq. (3.1) in the interval $(v_j, v)$. Let $f(v) = -\frac{b(2m+n)}{c(2m-n)} + \frac{a(2m+n)}{2cm}v + v^2$. Applying the change of variable $m = \frac{\mu n}{2}$, the function becomes $f(v) = -\frac{b(\mu+1)}{c(\mu-1)} + \frac{a(\mu+1)}{c\mu}v + v^2$. The discriminant is given by $\bar{\Delta} = \frac{(1+\mu)}{c^2}\left(\frac{4bc}{-1+\mu} + \frac{a^2(1+\mu)}{\mu^2}\right)$, and the roots are $v_K = -\frac{a(1+\mu)+c\mu\sqrt{\bar{\Delta}}}{2c\mu}$ and $v_L = -\frac{a(1+\mu)-c\mu\sqrt{\bar{\Delta}}}{2c\mu}$. The equation $\bar{\Delta} = 0$ has the roots $\mu = -\mu_1 = -\frac{a}{\sqrt{\Delta}}$ and $\mu = \mu_1 = \frac{a}{\sqrt{\Delta}}$. For the existence of solutions, it is required that $\mu \neq 0$ and $\mu \neq \pm 1$.

1. Let $a > 0$, $b > 0$, $c > 0$, and $p > 0$. For $\bar{\Delta} > 0$ and $|\mu| > 1$, there exists a closed periodic orbit that intersects the $v$-axis at $(v_L, 0)$ and approaches the origin (see Figure 5a). By choosing this closed curve as the integral path, we obtain

   $$\int_0^v \frac{dv}{\sqrt{v(v - v_K)(v_L - v)}} = \pm\sqrt{\frac{2n^2c}{mp|2m+n|}}(\xi - \xi_0),$$

   where $v_K < 0 < v_L$. It gives rise to the following exact solution of (3.1):

   $$v(\xi) = \frac{v_K v_L \operatorname{sn}^2\left(\Omega_1(\xi - \xi_0), m_1\right)}{v_K - v_L + v_L \operatorname{sn}^2\left(\Omega_1(\xi - \xi_0), m_1\right)},$$

   where

   $$\Omega_1 = \sqrt{\frac{n^2c(v_L - v_K)}{2mp|2m+n|}}, \quad m_1 = \sqrt{\frac{v_L}{v_L - v_K}}.$$

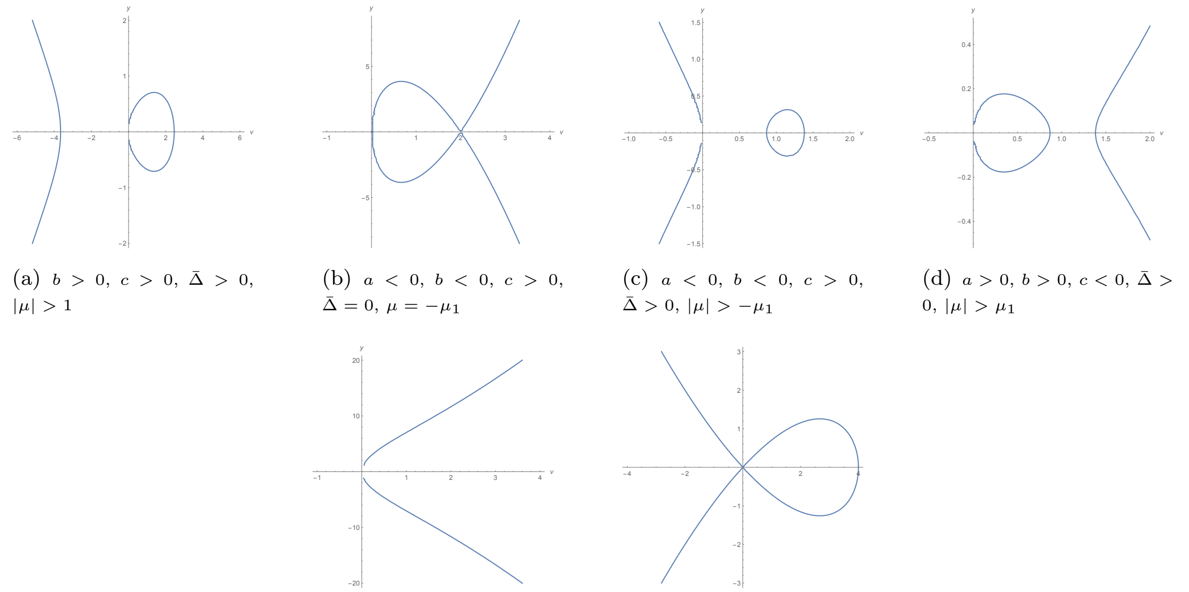

(a) $b > 0$, $c > 0$, $\bar{\Delta} > 0$, $|\mu| > 1$

(b) $a < 0$, $b < 0$, $c > 0$, $\bar{\Delta} = 0$, $\mu = -\mu_1$

(c) $a < 0$, $b < 0$, $c > 0$, $\bar{\Delta} > 0$, $|\mu| > -\mu_1$

(d) $a > 0, b > 0, c < 0, \bar{\Delta} > 0$, $|\mu| > \mu_1$

(e) $a < 0, b < 0, c < 0, \bar{\Delta} < 0$, $1 > \mu > -\mu_1$

(f) $a < 0$, $c > 0$, $b = 0$, $\mu > 0$ or $\mu < -1$

**Figure 5.** The level curves defined by Eq. (3.6) for $h = 0$, $p > 0$, and $m = \frac{\mu n}{2}$.

Therefore, we obtain the following periodic wave solutions of (2.5):

$$\psi(\xi) = \left( \frac{v_K v_L \,\mathrm{sn}^2\big(\Omega_1(\xi - \xi_0), m_1\big)}{v_K - v_L + v_L \mathrm{sn}^2\big(\Omega_1(\xi - \xi_0), m_1\big)} \right)^{\frac{1}{n}}. \tag{3.8}$$

For $\bar{\Delta} = 0$, there exist two homoclinic orbits asymptotically approaching the origin: One of them intersects the horizontal axis at $(v_K, 0)$ for $\mu = \mu_1$, while the other intersects at $(v_L, 0)$ for $\mu = -\mu_1$ (see Figure 5b). By choosing this homoclinic orbit as the integral path, Eq. (3.7) becomes

$$\int_0^v \frac{dv}{(v_L - v)\sqrt{v}} = \pm\sqrt{\frac{2n^2 c}{mp\,|2m+n|}}(\xi - \xi_0),$$

where $v_L > 0$. This leads to the parametric representation of a dark solitary wave solution of (3.1), which is given by

$$v(\xi) = v_L \tanh^2[\sqrt{\frac{v_L c n^2}{2mp|2m+n|}}(\xi - \xi_0)].$$

Therefore, we obtain the following exact dark solitary wave solution of Eq. (2.5):

$$\psi(\xi) \; = \left( v_L \mathrm{tanh}^2[\sqrt{\frac{v_L c n^2}{2mp|2m+n|}}(\xi - \xi_0)] \;\right)^{\frac{1}{n}}. \tag{3.9}$$

2. Let $a < 0$, $b < 0$, $c > 0$, and $p > 0$. For $\bar{\Delta} > 0$ and $|\mu| > -\mu_1$, there exists a periodic orbit, centered at $E_1(v_1, 0)$, which intersects the horizontal axis at the points $(v_K, 0)$ and $(v_L, 0)$ (see Figure 5c). When $0 < \mu < 1$, a closed orbit occurs that intersects the horizontal axis at $(v_L, 0)$ and tends toward the origin. Choosing the periodic orbit as the integration path, Eq. (3.7) can be rewritten as

$$\int_{v_K}^{v} \frac{dv}{\sqrt{v(v-v_K)(v_L-v)}} = \pm\sqrt{\frac{2n^2c}{mp|2m+n|}}(\xi-\xi_0),$$

where $0 < v_K < v_1 < v_L$. From this relation, we obtain the parametric representation of the family of periodic solutions of (3.1) given by

$$v(\xi) = \frac{v_K v_L}{v_L - (v_L - v_K)\operatorname{sn}^2(\Omega_2(\xi-\xi_0), m_2)},$$

where

$$\Omega_2 = \sqrt{\frac{v_L n^2 c}{2mp|2m+n|}}, \quad m_2 = \sqrt{\frac{v_L - v_K}{v_L}}.$$

Thus, we get the following periodic wave solutions of Eq. (2.5):

$$\psi(\xi) = \left(\frac{v_K v_L}{v_L - (v_L - v_K)\operatorname{sn}^2(\Omega_2(\xi-\xi_0), m_2)}\right)^{\frac{1}{n}}. \tag{3.10}$$

3. Let $a > 0$, $b > 0$, $c < 0$, and $p > 0$. For $\bar{\Delta} > 0$ and $|\mu| > \mu_1$, there exists a closed orbit that intersects the horizontal axis at the point $(v_K, 0)$ and tends toward the origin (see Figure 5d). When $\bar{\Delta} = 0$, i.e., $|\mu| = \mu_1$, a homoclinic orbit emerges that intersects the axis at the point $E_2(v_2, 0)$ and approaches the origin.
If the solution corresponding to the closed periodic orbit is chosen, then from Eq. (3.1) we obtain

$$\int_{0}^{v} \frac{dv}{\sqrt{v(v_K-v)(v_L-v)}} = \pm\sqrt{\frac{-2n^2c}{mp|2m+n|}}(\xi-\xi_0),$$

where $0 < v_K < v_L$. From this, we derive the parametric representation of the family of periodic solutions of Eq. (3.1) given by

$$v(\xi) = v_K \operatorname{sn}^2\left(\sqrt{\frac{-v_L n^2 c}{2mp|2m+n|}}(\xi-\xi_0), \sqrt{\frac{v_K}{v_L}}\right).$$

Accordingly, the periodic wave solutions of Eq. (2.5) is given by

$$\psi(\xi) = \left(v_K \operatorname{sn}^2\left(\sqrt{\frac{-v_L n^2 c}{2mp|2m+n|}}(\xi-\xi_0), \sqrt{\frac{v_K}{v_L}}\right)\right)^{\frac{1}{n}}. \tag{3.11}$$

4. Let $a < 0$, $b < 0$, $c < 0$, and $p > 0$. For $\bar{\Delta} > 0$ and $|\mu| > -\mu_1$, a closed periodic orbit appears that intersects the horizontal axis at $(v_K, 0)$ and tends toward the origin. For $|\mu| < -\mu_1$, there exists a periodic orbit centered at $E_1(v_1, 0)$. For $\bar{\Delta} < 0$ and $-\mu_1 < |\mu| < 1$, an unbounded orbit exists that comes from infinity and approach the origin (see Figure 5e).

By choosing this unbounded orbit as the integral path, we obtain

$$\int_0^v \frac{dv}{\sqrt{v[(v-b_1)^2+a_1^2]}} = \pm\sqrt{\frac{-2n^2c}{mp|2m+n|}}(\xi-\xi_0).$$

From this, we obtain the parametric representation of Eq. (3.1) given by

$$v(\xi) = \frac{A(1-\mathrm{cn}(\Omega_3(\xi-\xi_0),m_2))}{1+\mathrm{cn}(\Omega_3(\xi-\xi_0),m_2)},$$

where $A^2 = a_1^2 + b_1^2$, $\quad m_2 = \sqrt{\frac{A+b_1}{2A}}$, $\quad \Omega_3 = \sqrt{\frac{-2An^2c}{mp|2m+n|}}$. Thus, the solution of Eq. (2.5) is

$$\psi(\xi) = \left(\frac{A(1-\mathrm{cn}(\Omega_3(\xi-\xi_0),m_2)}{1+\mathrm{cn}(\Omega_3(\xi-\xi_0),m_2))}\right)^{\frac{1}{n}}. \tag{3.12}$$

5. Let $a < 0$, $b = 0$, $c > 0$, and $p > 0$. For $|2\mu+1| > 1$ a homoclinic orbit emerges that intersects the horizontal axis at $(v_L, 0)$ and tends toward the origin (see Figure 5f). For $v_L > 0$, the solution corresponding to the homoclinic trajectory is given by

$$\int_v^{v_L} \frac{dv}{v\sqrt{v_L - v}} = \sqrt{\frac{2n^2c}{mp|2m+n|}}(\xi-\xi_0),$$

and consequently the parametric representation of a bright solitary wave solution of Eq. (3.1) is

$$v(\xi) = v_L\,\mathrm{sech}^2\left(\sqrt{\frac{v_L n^2 c}{2mp|2m+n|}}(\xi-\xi_0)\right).$$

Hence, the exact bright solitary wave solution of Eq. (2.5) can be expressed as:

$$\psi(\xi) = \left(v_L\mathrm{sech}^2(\sqrt{\frac{v_L n^2 c}{2mp|2m+n|}}(\xi-\xi_0)\right)^{\frac{1}{n}}. \tag{3.13}$$

6. Let $a = 0$, $b > 0$, $c > 0$, and $p > 0$. For $|\mu| > 1$, closed orbits arise that intersect the horizontal axis at $(v_L, 0)$ and approach the origin (see Figure 5a).
For these orbits, assuming $v_L = -v_K$, the solution based on the integral

$$\int_0^v \frac{dv}{\sqrt{v(v+v_L)(v_L-v)}} = \pm\sqrt{\frac{2n^2c}{mp|2m+n|}}(\xi-\xi_0),$$

leads to the parametric representation of the family of periodic solutions of Eq. (3.1) given by

$$v(\xi) = \frac{v_L\,\mathrm{sn}^2\left(\Omega_4(\xi-\xi_0),\frac{1}{\sqrt{2}}\right)}{1+\mathrm{cn}^2\left(\Omega_4(\xi-\xi_0),\frac{1}{\sqrt{2}}\right)},$$

where $\Omega_4 = \sqrt{\frac{v_L n^2 c}{mp|2m+n|}}$. Hence, we obtain the following exact periodic wave solutions of Eq. (2.5):

$$\psi(\xi) = \left(\frac{v_L\,\mathrm{sn}^2\left(\Omega_4(\xi-\xi_0),\frac{1}{\sqrt{2}}\right)}{1+\mathrm{cn}^2\left(\Omega_4(\xi-\xi_0),\frac{1}{\sqrt{2}}\right)}\right)^{\frac{1}{n}}. \tag{3.14}$$

### 3.2. The exact traveling wave solutions of Eq. (2.5) with $h \neq 0$

In this section, we analyze all possible exact solutions of Eq. (2.5) by examining the phase portraits of system (3.4) in the case $h \neq 0$.

1. For $m = -n$, Eq. (3.3) can be rewritten as

$$y^2 = \frac{-2h}{p}\left(-\frac{b}{3h}\,v + \frac{a}{2h}\,v^2 + \frac{c}{h}\,v^3 + v^4\right), \qquad h \neq 0. \tag{3.15}$$

Integrating the first equation of system (3.2) by using Eq. (3.15), we obtain

$$\int_{v_j}^{v} \frac{dv}{\sqrt{\eta\left(-\frac{b}{3h}v + \frac{a}{2h}v^2 + \frac{c}{h}v^3 + v^4\right)}} = \pm\sqrt{2\left|\frac{h}{p}\right|}(\xi - \xi_0), \tag{3.16}$$

where $\eta = -sgn(hp)$. Now we assume that $0, v_K, v_L, v_M$ are the roots of the polynomial $g(v) = -\frac{b}{3h}v + \frac{a}{2h}v^2 + \frac{c}{h}v^3 + v^4$. These roots are then used to construct the solutions obtained from Eq. (3.16). From Eq. (3.3), the values of $H(v_i, 0) = h_i$ for the level curves $H(v, y) = h$ are given by

$$H(v_i, 0) = v_i^{-3}\left(\frac{b}{3} - \frac{a}{2}v_i - cv_i^2\right) = h_i. \tag{3.17}$$

In the following, for the case $\Delta > 0$, $p > 0$, and $n < 0$, the parametric solutions of Eq. (2.5) are determined by using the level curves Eq. (3.15) given in Figure 6.

(a) When $c > 0$.

i. For $a > 0$ and $b > 0$, we have $v_1 < 0 < v_2$. In this case, the equilibrium point $E_1(v_1, 0)$ is a center, and $E_2(v_2, 0)$ is a saddle.

- For $h = h_2 < 0 < h_1$, the level curves $H(v, y) = h$ admit a homoclinic orbit passing through the saddle point $E_2(v_2, 0)$ and approaching the origin, as shown in Figures 1a and 6a. Taking this homoclinic orbit as the integration path, Eq. (3.16) becomes

$$\int_0^v \frac{dv}{(v_2 - v)\sqrt{(v - v_K)v}} = \pm\sqrt{\frac{-2h}{p}}(\xi - \xi_0),$$

where $v_K < 0 < v_2$. From this, the solution of Eq. (3.1) becomes:

$$v(\xi) = v_2 + \frac{2v_2(v_2 - v_K)}{v_K - 2v_2 + v_K\cosh(\omega_1(\xi - \xi_0))},$$

where

$$\omega_1 = \sqrt{\frac{2v_2(v_K - v_2)h}{p}}.$$

Hence, we can obtain the following dark solitary wave solution of Eq. (2.5)

$$\psi(\xi) = \left(v_2 + \frac{2v_2(v_2 - v_K)}{v_K - 2v_2 + v_K\cosh(\omega_1(\xi - \xi_0))}\right)^{1/n}. \tag{3.18}$$

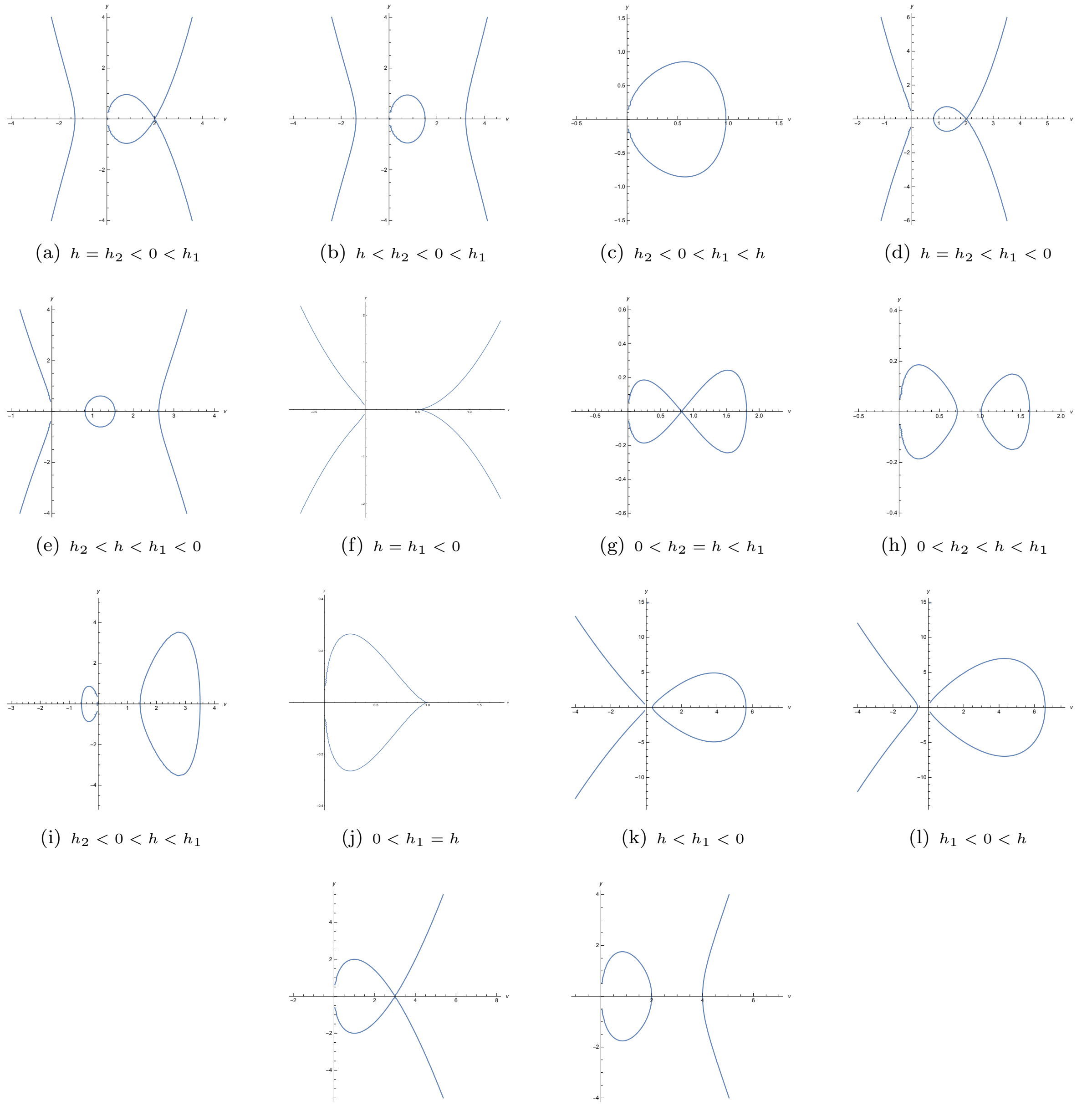

(a) $h = h_2 < 0 < h_1$ (b) $h < h_2 < 0 < h_1$ (c) $h_2 < 0 < h_1 < h$ (d) $h = h_2 < h_1 < 0$

(e) $h_2 < h < h_1 < 0$ (f) $h = h_1 < 0$ (g) $0 < h_2 = h < h_1$ (h) $0 < h_2 < h < h_1$

(i) $h_2 < 0 < h < h_1$ (j) $0 < h_1 = h$ (k) $h < h_1 < 0$ (l) $h_1 < 0 < h$

(m) $0 < h_1 = h$ (n) $0 < h_1 < h$

**Figure 6.** The variations of the level curves defined by $H(v, y) = h$ in system (3.4) for $\Delta > 0$, $p > 0$, and $n < 0$.

- For $h < h_2 < 0 < h_1$, the level curves $H(v, y) = h$ intersect the horizontal axis at $(v_L, 0)$ and form closed orbits approaching the origin, as shown in Figures 1a and 6b. The corresponding solution $v(\xi)$ is be obtained from Eq. (3.16) as:

$$\int_0^v \frac{dv}{\sqrt{(v - v_K)v(v_L - v)(v_M - v)}} = \pm\sqrt{\frac{-2h}{p}}(\xi - \xi_0),$$

where $v_K < 0 < v_L < v_M$. From this, we obtain the parametric representation of the family of periodic solutions of Eq. (3.1) given by

$$v(\xi) = \frac{v_K v_L \,\mathrm{sn}^2(\omega_2(\xi - \xi_0), k_1)}{v_K - v_L + v_L \,\mathrm{sn}^2(\omega_2(\xi - \xi_0), k_1)},$$

where

$$\omega_2 = \sqrt{\frac{h v_M (v_K - v_L)}{2p}}, \quad k_1 = \sqrt{\frac{v_L(v_M - v_K)}{v_M(v_L - v_K)}}.$$

Thus, the exact periodic wave solutions of Eq. (2.5) is:

$$\psi(\xi) = \left(\frac{v_K v_L \,\mathrm{sn}^2(\omega_2(\xi - \xi_0), k_1)}{v_K - v_L + v_L \,\mathrm{sn}^2(\omega_2(\xi - \xi_0), k_1)}\right)^{1/n}. \tag{3.19}$$

- For $h_2 < 0 < h_1 < h$, the level curves $H(v, y) = h$ intersect the horizontal axis at $(v_L, 0)$ and form periodic orbits approaching the origin, as shown in Figures 1a and 6c. When the periodic orbit is chosen as the integration path, Eq. (3.16) becomes

$$\int_0^v \frac{dv}{\sqrt{v(v_L - v)[(v - b_1)^2 + a_1^2]}} = \pm\sqrt{\frac{2h}{p}}(\xi - \xi_0),$$

where $0 < v_L < v_2$. From this, we derive the parametric representation of the family of periodic solutions of Eq. (3.1) given by

$$v(\xi) = \frac{B v_L (1 - \mathrm{cn}(\omega_3 \xi, k_2))}{A + B + (A - B)\mathrm{cn}(\omega_3 \xi, k_2)},$$

where $\omega_3 = \sqrt{\frac{2ABh}{p}}$, $k_2 = \sqrt{\frac{v_L^2 - (A-B)^2}{4AB}}$, $A^2 = (v_L - b_1)^2 + a_1^2$, $B^2 = b_1^2 + a_1^2$. Therefore, the exact periodic wave solutions of Eq. (2.5) is:

$$\psi(\xi) = \left(\frac{B v_L (1 - \mathrm{cn}(\omega_3(\xi - \xi_0), k_2))}{A + B + (A - B)\mathrm{cn}(\omega_3(\xi - \xi_0), k_2)}\right)^{1/n}. \tag{3.20}$$

ii. For $a < 0$, $b < 0$, we have $0 < v_1 < v_2$. In this case, the equilibrium point $E_1(v_1, 0)$ is a center, while $E_2(v_2, 0)$ is a saddle point.

- For $h = h_2 < h_1 < 0$, the level curve $H(v, y) = h$ intersects the horizontal axis at the point $E_2(v_2, 0)$ and forms a homoclinic orbit that approaches the point $(v_L, 0)$ as shown in Figure 1c and 6d. Choosing a homoclinic orbit as the integral path, Eq. (3.16) becomes

$$\int_{v_L}^v \frac{dv}{(v_2 - v)\sqrt{(v - v_L)v}} = \pm\sqrt{\frac{-2h}{p}}(\xi - \xi_0),$$

where $0 < v_L < v_2$. This leads to the dark solitary wave solution:

$$v(\xi) = \frac{v_2 v_L}{v_L + (v_2 - v_L)\mathrm{sech}^2(\omega_4(\xi - \xi_0))},$$

where

$$\omega_4 = \sqrt{\frac{(v_L - v_2)v_2 h}{2p}}.$$

Thus, the dark solitary wave solution of Eq. (2.5) is

$$\psi(\xi) = \left( \frac{v_2 v_L}{v_L + (v_2 - v_L)\operatorname{sech}^2(\omega_4(\xi - \xi_0))} \right)^{\frac{1}{n}}. \tag{3.21}$$

- For $h_2 < h < h_1 < 0$, the level curves $H(v, y) = h$ intersect the horizontal axis at the points $(v_K, 0)$ and $(v_L, 0)$ and form a closed orbit surrounding the equilibrium point $E_1(v_1, 0)$ (see Figures 1c and 6e). Choosing the closed curve as the integral path, Eq. (3.16) becomes

$$\int_v^{v_L} \frac{dv}{\sqrt{v(v - v_K)(v_L - v)(v_M - v)}} = \pm\sqrt{\frac{-2h}{p}}(\xi - \xi_0),$$

where $0 < v_K < v_1 < v_L < v_M$.
This leads to the parametric representation of the family of periodic solutions:

$$v(\xi) = \frac{v_L(v_M - v_K) + v_M(v_K - v_L)sn^2(\omega_5\xi, k_3)}{v_M - v_K + (v_K - v_L)sn^2(\omega_5\xi, k_3)},$$

with the coefficients:

$$\omega_5 = \sqrt{\frac{hv_L(v_K - v_M)}{2p}}, \quad k_3 = \sqrt{\frac{v_M(v_L - v_K)}{(v_M - v_K)v_L}}.$$

Thus, the exact periodic wave solutions of Eq. (2.5) becomes

$$\psi(\xi) = \left( \frac{v_L(v_M - v_K) + v_M(v_K - v_L)sn^2(\omega_5(\xi - \xi_0), k_3)}{v_M - v_K + (v_K - v_L)sn^2(\omega_5(\xi - \xi_0), k_3)} \right)^{\frac{1}{n}}. \tag{3.22}$$

iii. For $a < 0$, $b < 0$, the level curves $H(v, y) = h = h_1$ form two unbounded trajectories intersecting the $v$-axis at the cusp point $E_1(v_1, 0)$ (see Figures 1d and 6f). The corresponding trajectory solution $v = v(\xi)$ is given by:

$$\int_v^{\infty} \frac{dv}{(v - v_1)\sqrt{v(v - v_1)}} = \pm\sqrt{\frac{-2h}{p}}(\xi - \xi_0).$$

This leads to the solution

$$v(\xi) = \frac{v_1 \left(\omega_6(\xi - \xi_0) \pm 1\right)^2}{\omega_6(\xi - \xi_0) \left(\omega_6(\xi - \xi_0) \pm 2\right)},$$

where $\omega_6 = v_1\sqrt{\frac{-h}{2p}}$. Hence, the singular rational solutions of Eq. (2.5) are given by

$$\psi(\xi) = \left( \frac{v_1 \left(\omega_6(\xi - \xi_0) \pm 1\right)^2}{\omega_6(\xi - \xi_0) \left(\omega_6(\xi - \xi_0) \pm 2\right)} \right)^{\frac{1}{n}}. \tag{3.23}$$

(b) Let $c < 0$.

i. For $a > 0$ and $b > 0$, we have $0 < v_2 < v_1$. In this case, the equilibrium point $E_1(v_1, 0)$ is a center, while $E_2(v_2, 0)$ is a saddle point.

- For $0 < h_2 = h < h_1$, the level curve $H(v,y) = h$ intersects the $v$–axis at $(0,0)$, $(v_2,0)$, and $(v_M,0)$, giving rise to a separatrix consisting of two homoclinic orbits (see Figures 2a and 6g). For the first homoclinic orbit, with $0 < v_2 < v_1 < v_M$, the solution is obtained from the integral

$$\int_{v}^{v_M} \frac{dv}{(v-v_2)\sqrt{(v_M-v)v}} = \pm\sqrt{\frac{2h}{p}}(\xi-\xi_0),$$

which yields:

$$v(\xi) = \frac{v_2 v_M}{v_M - (v_M - v_2)\operatorname{sech}^2(\omega_7(\xi-\xi_0))},$$

where $\omega_7 = \sqrt{\frac{hv_2(v_M-v_2)}{2p}}$. The corresponding bright solitary wave solution of Eq. (2.5) is

$$\psi(\xi) = (\frac{v_2 v_M}{v_M - (v_M - v_2)\operatorname{sech}^2(\omega_7(\xi-\xi_0))})^{\frac{1}{n}}. \tag{3.24}$$

For the second homoclinic orbit, the solution is obtained from

$$\int_{0}^{v} \frac{dv}{(v_2-v)\sqrt{(v_M-v)v}} = \sqrt{\frac{2h}{p}}(\xi-\xi_0),$$

and is given by

$$v(\xi) = v_M - \frac{v_M(v_M-v_2)}{v_M + v_2\operatorname{sech}^2(\omega_7(\xi-\xi_0))}.$$

The corresponding dark solitary wave solution of Eq. (2.5) is

$$\psi(\xi) = (v_M - \frac{v_M(v_M-v_2)}{v_M + v_2\operatorname{sech}^2(\omega_7(\xi-\xi_0))})^{\frac{1}{n}}. \tag{3.25}$$

- For $0 < h_2 < h < h_1$, the level curves $H(v,y) = h$ form two distinct periodic orbits: The first intersects the horizontal axis at $(v_L,0)$ and $(v_M,0)$, enclosing the equilibrium point $(v_1,0)$ while the second passes through $(v_3,0)$ and is tangent to the singular point at the origin (see Figures 2a and 6h).
Choosing the periodic orbit centered at $(v_1,0)$ as the integral path, the solution $v = v(\xi)$ is obtained from

$$\int_{v_L}^{v} \frac{dv}{\sqrt{v(v-v_K)(v-v_L)(v_M-v)}} = \pm\sqrt{\frac{2h}{p}}(\xi-\xi_0),$$

where $0 < v_K < v_L < v_1 < v_M$. From this, we obtain the parametric representation of the family of periodic solutions of Eq. (3.1) given by

$$v(\xi) = \frac{v_L(v_M-v_K) - v_K(v_M-v_L)\operatorname{sn}^2(\omega_8(\xi-\xi_0),k_4)}{v_M - v_K - (v_M-v_L)\operatorname{sn}^2(\omega_8(\xi-\xi_0),k_4)},$$

where $\omega_8 = \sqrt{\frac{hv_L(v_M-v_K)}{2p}}$ and $k_4 = \sqrt{\frac{v_K(v_M-v_L)}{(v_M-v_K)v_L}}$. Hence, we obtain the following exact periodic wave solutions of Eq. (2.5):

$$\psi(\xi) = \left(\frac{v_L(v_M-v_K) - v_K(v_M-v_L)\operatorname{sn}^2(\omega_8(\xi-\xi_0),k_4)}{v_M - v_K - (v_M-v_L)\operatorname{sn}^2(\omega_8(\xi-\xi_0),k_4)}\right)^{\frac{1}{n}}. \tag{3.26}$$

On the other hand, choosing the second closed curve as the integral path, Eq. (3.16) becomes

$$\int_0^v \frac{dv}{\sqrt{v(v_K - v)(v_L - v)(v_M - v)}} = \pm\sqrt{\frac{2h}{p}}(\xi - \xi_0).$$

It gives rise to the following family of periodic solutions:

$$v(\xi) = \frac{v_K v_M \operatorname{sn}^2(\omega_8 \xi, k_4)}{v_M - v_K + v_K \operatorname{sn}^2(\omega_8 \xi, k_4)}.$$

Hence, we derive the exact periodic wave solutions of Eq. (2.5):

$$\psi(\xi) = \left(\frac{v_K v_M \operatorname{sn}^2(\omega_8(\xi - \xi_0), k_4)}{v_M - v_K + v_K \operatorname{sn}^2(\omega_8(\xi - \xi_0), k_4)}\right)^{\frac{1}{n}}. \tag{3.27}$$

ii. For $a < 0$ and $b > 0$, we have $v_2 < v_1 < 0$. In this case, the equilibrium point $E_1(v_1, 0)$ is a center, while $E_2(v_2, 0)$ is a saddle point (see Figures 2b and 6c).
For $h_2 < 0 < h_1 < h$, the level curves $H(v, y) = h$ obtained from equation (3.17) intersect the horizontal axis at $(v_M, 0)$, forming closed periodic orbits approaching the origin. The corresponding solution $v = v(\xi)$, obtained from Eq. (3.16), is similar to Eq. (3.20).

iii. For $a < 0$ and $b < 0$, we have $v_2 < 0 < v_1$. In this case, the equilibrium point $E_1(v_1, 0)$ is a center, while $E_2(v_2, 0)$ is a saddle point, as shown in Figures 2c and 6i.
For $h_2 < 0 < h < h_1$, the level curves $H(v, y) = h$ obtained from equation (3.17) form a periodic orbit centered at $(v_1, 0)$, intersecting the horizontal axis at the points $(v_L, 0)$ and $(v_M, 0)$. By selecting the periodic orbit as the integration path, Eq. (3.16) takes the form

$$\int_{v_L}^v \frac{dv}{\sqrt{(v - v_K)v(v - v_L)(v_M - v)}} = \pm\sqrt{\frac{2h}{p}}(\xi - \xi_0),$$

where $v_K < 0 < v_L < v_1 < v_M$.
This solution is given by

$$v(\xi) = \frac{v_M v_L}{v_M - (v_M - v_L)\operatorname{sn}^2(\omega_9(\xi - \xi_0), k_5)},$$

where the constants are defined as

$$\omega_9 = \sqrt{\frac{v_M(v_L - v_K)h}{2p}}, \quad k_5 = \sqrt{\frac{v_K(v_L - v_M)}{(v_L - v_K)v_M}}.$$

Thus, the exact periodic wave solution of Eq. (2.5) is

$$\psi(\xi) = \left(\frac{v_M v_L}{v_M - (v_M - v_L)\operatorname{sn}^2(\omega_9(\xi - \xi_0), k_5)}\right)^{\frac{1}{n}}. \tag{3.28}$$

iv. For $a > 0$, $b > 0$ we have $0 < v_1 = v_2$. In this case, the equilibrium point of the system becomes a cusp. Accordingly, the level curves $H(v, y) = h = h_1$ form a homoclinic trajectory that intersects the horizontal axis at $E_1(v_1, 0)$ and approaches the origin. (see

Figures 2d and 6j). The corresponding solution $v = v(\xi)$ for homoclinic orbit is given by:

$$\int_0^v \frac{dv}{(v_1 - v)\sqrt{v(v_1 - v)}} = \pm\sqrt{\frac{2h}{p}}(\xi - \xi_0).$$

Then we have

$$v(\xi) = \frac{v_1\,(\omega_{10}(\xi - \xi_0))^2}{4 + (\omega_{10}(\xi - \xi_0))^2},$$

where $\omega_{10} = v_1\sqrt{\frac{h}{2p}}$. Thus, equation (2.5) admits a dark solitary wave solution of the form

$$\psi(\xi) = (\frac{v_1\,(\omega_{10}(\xi - \xi_0))^2}{4 + (\omega_{10}(\xi - \xi_0))^2})^{\frac{1}{n}}. \tag{3.29}$$

2. For the case $b = 0$, $p > 0$, and $n > 0$, the solutions satisfying Eq. (2.5) are obtained from the phase portraits of system (3.4). In this case, for $n = 2m$, Eq. (3.3) becomes

$$y^2 = \begin{cases} \dfrac{2c}{p}\left(\dfrac{2h}{c}v - \dfrac{2a}{c}v^2 - v^3\right), & c > 0, \\ \dfrac{-2c}{p}\left(-\dfrac{2h}{c}v + \dfrac{2a}{c}v^2 + v^3\right), & c < 0. \end{cases} \tag{3.30}$$

Integrating the first equation of system (3.2) over the interval $(v_j, v)$ by using Eq. (3.30), we obtain

$$\int_{v_j}^v \frac{dv}{\sqrt{\eta_1 v\left(-\frac{2h}{c} + \frac{2a}{c}v + v^2\right)}} = \pm\sqrt{\frac{2|c|}{p}}(\xi - \xi_0), \tag{3.31}$$

where $\eta_1 = -sgn(c)$. To analyze the dynamical behavior of system (3.4), we assume that the real numbers 0, $v_L$, and $v_M$ are the roots of the polynomial $g_1(v) = -\frac{2h}{c}v + \frac{2a}{c}v^2 + v^3$. From Eq. (3.3), the level values for the curves $H(v_i, 0) = h_i$ are computed as

$$H(v_i, 0) = v_i\left(a + \frac{c}{2}v_i\right) = h_i. \tag{3.32}$$

(a) If $a > 0$ and $c > 0$, then the equilibrium point $E_1(v_1, 0)$ is a saddle. If $a < 0$ and $v_1 < 0$, then $E_1(v_1, 0)$ is a center, as shown in Figures 3b and 6k.

- For $h_1 < h < 0$, the level curves $H(v, y) = h$, obtained from equation (3.32), form a periodic orbit centered at $(v_1, 0)$ that intersects the horizontal axis at the points $(v_L, 0)$ and $(v_M, 0)$.
  For this orbit, the solution $v = v(\xi)$, derived from equation (3.31), is expressed from the integral

$$\int_{v_L}^v \frac{dv}{\sqrt{v(v - v_L)(v_M - v)}} = \pm\sqrt{\frac{2c}{p}}(\xi - \xi_0),$$

where $0 < v_L < v_1 < v_M$. This yields the periodic solution:

$$v(\xi) = \frac{v_L v_M}{v_M - (v_M - v_L)\,\mathrm{sn}^2\left(\omega_{11}(\xi - \xi_0), k_6\right)},$$

where the constants are defined as

$$\omega_{11} = \sqrt{\frac{cv_M}{2p}}, \quad k_6 = \sqrt{\frac{v_M - v_L}{v_M}}.$$

Thus, the exact periodic wave solution of Eq. (2.5) is

$$\psi(\xi) = \left( \frac{v_L v_M}{v_M - (v_M - v_L)\,\mathrm{sn}^2\left(\omega_{11}(\xi - \xi_0), k_6\right)} \right)^{\frac{1}{n}}. \tag{3.33}$$

- For $h_1 < 0 < h$, the level curves $H(v, y) = h$, again obtained from Eq. (3.32), form a closed trajectory passing through the origin and intersecting the horizontal axis at $(v_M, 0)$, as shown in Figures 3b-6l.

  The solution $v = v(\xi)$, derived from Eq. (3.31), is obtained from the integral

$$\int_0^v \frac{dv}{\sqrt{v(v - v_L)(v_M - v)}} = \pm\sqrt{\frac{2c}{p}}(\xi - \xi_0),$$

where $v_L < 0 < v_1 < v_M$. The solution is

$$v(\xi) = \frac{v_M v_L\,\mathrm{sn}^2(\omega_{12}(\xi - \xi_0), k_7)}{v_L - v_M + v_M\,\mathrm{sn}^2(\omega_{12}(\xi - \xi_0), k_7)},$$

with the constants

$$\omega_{12} = \sqrt{\frac{c(v_M - v_L)}{2p}}, \qquad k_7 = \sqrt{\frac{v_M}{v_M - v_L}}.$$

Thus, the singular periodic wave solution of Eq. (2.5) becomes

$$\psi(\xi) = \left( \frac{v_M v_L\,\mathrm{sn}^2(\omega_{12}(\xi - \xi_0), k_7)}{v_L - v_M + v_M\,\mathrm{sn}^2(\omega_{12}(\xi - \xi_0), k_7)} \right)^{\frac{1}{n}}. \tag{3.34}$$

(b) If $a > 0$ and $c < 0$, then the equilibrium point $E_1(v_1, 0)$ is a saddle. If $a < 0$ and $c < 0$, then $E_1(v_1, 0)$ is a center, as shown in Figure 3c.

- For $0 < h_1 = h$, the level curves defined by $H(v, y) = h$ admit a homoclinic orbit passing through the saddle point $(v_1, 0)$ and approaching the origin (see Figure 6m). Taking this homoclinic orbit as the integration path for $0 < v_1$, Eq. (3.31) becomes

$$\int_0^v \frac{dv}{(v_1 - v)\sqrt{v}} = \pm\sqrt{\frac{-2c}{p}}(\xi - \xi_0),$$

which yields

$$v(\xi) = v_1 \tanh^2\left( \sqrt{-\frac{v_1 c}{2p}}(\xi - \xi_0) \right).$$

Then,the exact dark solitary wave solution of Eq. (2.5) is

$$\psi(\xi) = \left( v_1 \tanh^2\left( \sqrt{-\frac{v_1 c}{2p}}(\xi - \xi_0) \right) \right)^{\frac{1}{n}}. \tag{3.35}$$

- For $0 < h_1 < h$, the level curves $H(v,y) = h$ form a closed trajectory, which intersects the horizontal axis at $(v_L, 0)$ and approaches the origin (see Figure 6n).
  Selecting $0 < v_L < v_1 < v_M$, the solution $v = v(\xi)$ is obtained from the integral

$$\int_0^v \frac{dv}{\sqrt{v(v_L - v)(v_M - v)}} = \pm\sqrt{\frac{-2c}{p}}(\xi - \xi_0),$$

  which gives the periodic solution

$$v(\xi) = v_L \operatorname{sn}^2\left(\sqrt{-\frac{v_M c}{2p}}(\xi - \xi_0), \sqrt{\frac{v_L}{v_M}}\right).$$

  Then the exact periodic wave solution of Eq. (2.5) becomes

$$\psi(\xi) = \left(v_L \operatorname{sn}^2\left(\sqrt{-\frac{v_M c}{2p}}(\xi - \xi_0), \sqrt{\frac{v_L}{v_M}}\right)\right)^{\frac{1}{n}}. \tag{3.36}$$

## 4. Bifurcation analysis and exact traveling wave solutions of Eq. (2.6)

In this section, we investigate the bifurcations of phase portraits of the reduced ordinary differential equation given by (2.6). First, making the transformation

$$\psi = v^{\frac{1}{n-m}}, \tag{4.1}$$

we obtain

$$\frac{mp(2m-n)}{(n-m)^2}(v')^2 + \frac{mp}{n-m}vv'' + av^2 - bv^3 + cv^4 = 0. \tag{4.2}$$

Eq. (4.2) can be transformed into the following two-dimensional system:

$$\frac{dv}{d\xi} = y, \qquad \frac{dy}{d\xi} = \frac{\frac{mp(n-2m)}{(n-m)^2}y^2 - av^2 + bv^3 - cv^4}{\frac{mp}{n-m}v}, \tag{4.3}$$

which has the first integral

$$H(v,y) = v^{\frac{2m}{n-m}-2}(n-m)\left(\frac{mp}{2(n-m)^2}y^2 + \frac{a}{2m}v^2 - \frac{b}{m+n}v^3 + \frac{c}{2n}v^4\right) = h, \tag{4.4}$$

where $h$ is an integral constant. The expression (4.4) yields the wave solutions that will be obtained from phase portraits in the following sections. Moreover, for the solutions of the singular dynamical system, it is required that $m \neq n$ and $n \neq 2m$. Apply $d\xi = \frac{mp}{n-m}vd\zeta$, the singular system (4.3) has the same invariant curve solutions as the associated regular system

$$\frac{dv}{d\zeta} = \frac{mp}{n-m}yv, \qquad \frac{dy}{d\zeta} = \frac{mp(n-2m)}{(n-m)^2}y^2 - av^2 + bv^3 - cv^4. \tag{4.5}$$

For the equilibrium points of this system, setting $y = 0$ and solving $v^2(-a + bv - cv^2) = 0$ yields the values $v_0 = 0$, $v_1 = \frac{b-\sqrt{b^2-4ac}}{2c}$, and $v_2 = \frac{b+\sqrt{b^2-4ac}}{2c}$. Therefore, the equilibrium points are $E_0(v_0, 0)$, $E_1(v_1, 0)$, and $E_2(v_2, 0)$.

The Jacobian matrix of system (4.5) is given by

$$M(v,y)=\begin{bmatrix}\dfrac{mp}{n-m}y & \dfrac{mp}{n-m}v\\ -2av+3bv^2-4cv^3 & \dfrac{2mp(n-2m)}{(n-m)^2}y\end{bmatrix}.$$

At the equilibrium point $E_i(v_i,0)$, the determinant of the Jacobian matrix becomes

$$J(v_i,0)=\frac{mp}{n-m}{v_i}^2(4c{v_i}^2-3bv_i+2a),$$

which can also be expressed in terms of the equilibrium components as

$$J(v_i,0)=\frac{cmp}{n-m}{v_i}^2\left[2(v_i-v_1)(v_i-v_2)+v_i(v_i-v_2)+v_i(v_i-v_1)\right].$$

From this, the determinant of the Jacobian matrix at the equilibrium points can be expressed as follows:

$$J_0(0,0)=0,\quad J_1(v_1,0)=\frac{cmp}{n-m}v_1^3(v_1-v_2),\quad J_2(v_2,0)=\frac{cmp}{n-m}v_2^3(v_2-v_1).$$

The analysis of the equilibrium points of system (4.5), along with the corresponding phase diagrams, is presented in Figures 7 and 8.

1. We assume that $\Delta_1=b^2-4ac>0$, $p>0$, and $n>m$.
   (a) For $c>0$, we have
      i. If $a>0$, $b>0$, then $0<v_1<v_2$, in which case $E_1(v_1,0)$ is a saddle and $E_2(v_2,0)$ is a center (see Figure 7a-c).
      ii. If $a<0$, then $v_1<0<v_2$, and both $E_1(v_1,0)$ and $E_2(v_2,0)$ are centers (see Figure 7d).
      iii. If $a>0$, $b<0$, then $v_1<v_2<0$, in which case $E_1(v_1,0)$ is a center and $E_2(v_2,0)$ is a saddle.
   (b) For $c<0$, we have
      i. If $a>0$, then $v_2<0<v_1$, so both $E_1(v_1,0)$ and $E_2(v_2,0)$ are saddles (see Figure 7e).
      ii. If $a<0$ and $b>0$, then $v_2<v_1<0$, in which case $E_1(v_1,0)$ is a saddle and $E_2(v_2,0)$ is a center.
      iii. If $a<0$, $b<0$, then $0<v_2<v_1$, and $E_1(v_1,0)$ is a center while $E_2(v_2,0)$ is a saddle (see Figure 7f-h).

   Depending on the sign of the parameter $p$ and the case $n<m$, the stability types of the equilibrium points interchange: The saddle points become centers, and the centers become saddles.

2. In the case $\Delta_1=b^2-4ac=0$, the equilibriums points are $E_0(0,0)$ and $E_1(v_1,0)$, where $v_1=v_2=\frac{b}{2c}$. Since $J(v_1,0)=0$, the point $E_1(v_1,0)$ is identified as a cusp point (see Figures 8a and 8b).

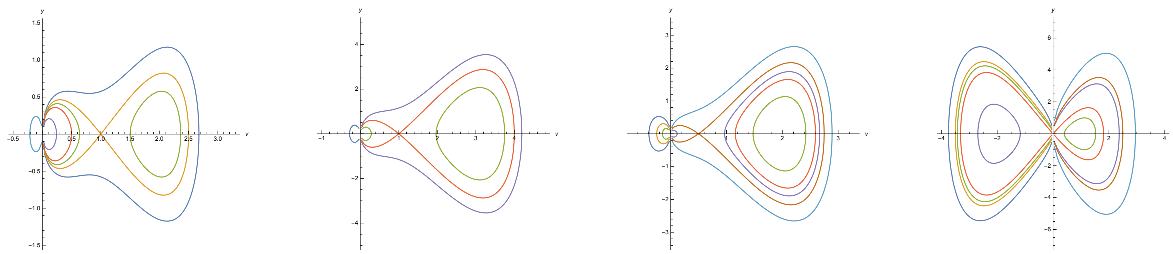

(a) $a > 0,\ b > 0,\ c > 0$ (b) $a > 0,\ b > 0,\ c > 0$ (c) $a > 0,\ b > 0,\ c > 0$ (d) $a < 0,\ b < 0,\ c > 0$

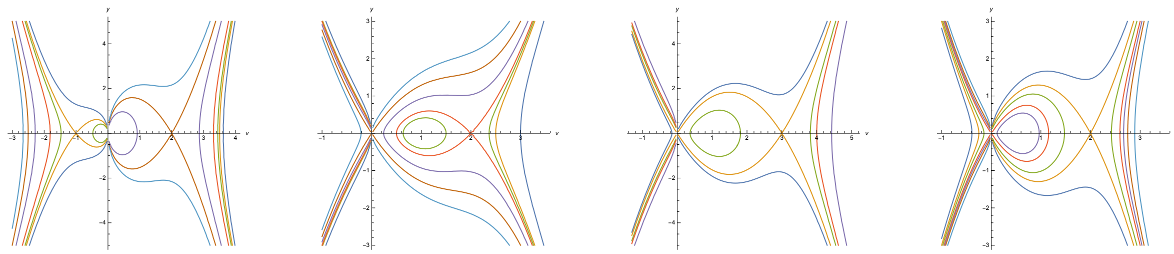

(e) $a > 0,\ b < 0,\ c < 0$ (f) $a < 0,\ b < 0,\ c < 0$ (g) $a < 0,\ b < 0,\ c < 0$ (h) $a < 0,\ b < 0,\ c < 0$

**Figure 7.** The phase portraits of system (4.5) for $p > 0$, $\Delta_1 > 0$, $mn > 0$.

3. We assume that $b = 0$, $p > 0$ and $n = -m$. In this case, system (4.5) has three equilibrium points

$$E(v_0, 0), \quad E_1(v_1, 0), \quad \text{and} \quad E_2(v_2, 0).$$

At the equilibrium points $E_i(v_i, 0)$, the determinant of the Jacobian matrix can be expressed as follows:

$$J_i(v_i, 0) = \frac{mp}{n-m} v_i^2 \left(4cv_i^2 + 2a\right) = \frac{-a^2 p}{c},$$

and a bifurcation analysis is performed based on these values.

(a) If $c > 0$ and $a < 0$, we have $v_1 < 0 < v_2$, and in this case, both $E_1(v_1, 0)$ and $E_2(v_2, 0)$ are saddle points (see Figure 8c).

(b) If $c < 0$ and $a > 0$, we also have $v_2 < 0 < v_1$, and in this case, both $E_1(v_1, 0)$ and $E_2(v_2, 0)$ are centers (see Figure 8d).

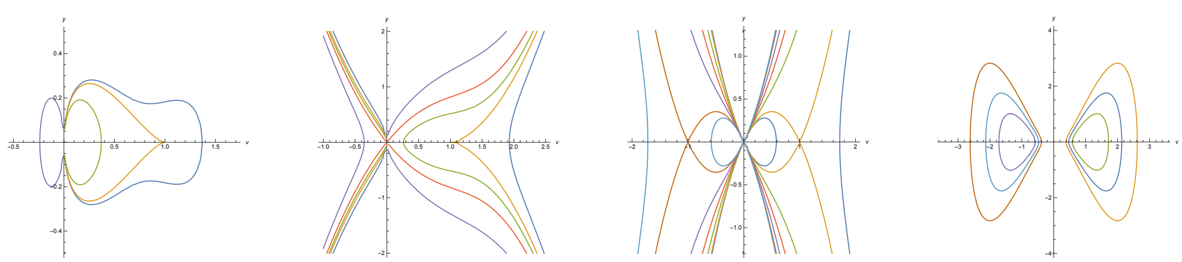

(a) $a > 0,\ b > 0,\ c > 0,\ mn > 0,\ \Delta_1 = 0$ (b) $a < 0,\ b < 0,\ c < 0,\ mn > 0,\ \Delta_1 = 0$ (c) $a < 0,\ b = 0,\ c > 0,\ mn < 0$ (d) $a > 0,\ b = 0,\ c < 0,\ mn < 0$

**Figure 8.** The phase portraits of system (4.5) for $p > 0$.

4. Depending on the sign of the parameter $p$, the stability of the equilibrium points interchanges: The points that are saddle become centers, and the centers become saddle points. In this case, the new phase portraits corresponding to the same structure are observed to be symmetric with respect to the original ones.

### 4.1. The exact traveling wave solutions of Eq. (2.6) given by the level curves H(v,y)=0

In this section, we consider the possible exact travel wave solution of Eq. (2.6) by using the first equation of system (4.4) and Eq. (4.5).

By substituting $h = 0$ into Eq. (4.4) and assuming $b \neq 0$, and $p > 0$, Eq. (4.4) reduces to the following form:

$$y^2 = \frac{(n-m)^2}{mp}\left(-\frac{a}{m}v^2 + \frac{2b}{m+n}v^3 - \frac{c}{n}v^4\right). \tag{4.6}$$

By substituting the square root of Eq. (4.6) into the first equation of system (4.3) and integrating the result over the interval $(v_j, v)$, one obtains

$$\int_{v_j}^{v} \frac{dv}{\sqrt{\frac{v^2}{p}\left(-\frac{a}{m} + \frac{2b}{m+n}v - \frac{c}{n}v^2\right)}} = \pm\frac{|n-m|}{\sqrt{m}}(\xi - \xi_0), \tag{4.7}$$

where $v = v(\xi)$ is the solution of the Eq. (4.2). Let $n = \frac{\mu+1}{\mu}m$. Then the discriminant of the function

$$f_1(v) = -\frac{a(\mu+1)}{c\mu} + \frac{2b(\mu+1)}{c(2\mu+1)}v - v^2,$$

is given by

$$\overline{\Delta}_1 = \frac{4(\mu+1)}{c^2}\left(-\frac{ac}{\mu} + \frac{b^2(\mu+1)}{(2\mu+1)^2}\right).$$

Let the roots of the equation $f_1(v) = 0$ be denoted by $v_K$ and $v_L$. The values of $\mu$ that satisfy $\overline{\Delta}_1 = 0$ are

$$\mu_1 = -\frac{1}{2} - \frac{b^2}{2\sqrt{b^4 - 4ab^2c}}, \quad \mu_2 = -\frac{1}{2} + \frac{b^2}{2\sqrt{b^4 - 4ab^2c}}.$$

For the existence of the solution, it is necessary that $\mu \neq 0, \mu \neq -0.5,$ and $\mu \neq -1$. Using (4.7), under some special parametric conditions, we can obtain the explicit parametric representations for the solutions of system (4.5).

1. Let $a > 0$, $c > 0$, and $\overline{\Delta}_1 > 0$. For $\mu > \mu_2$ or $\mu < \mu_1$, the system exhibits periodic orbits: They occur on the right side of the phase plane if $b > 0$ (see Figure 9a), and on the left side if $b < 0$. Moreover, in the interval $-1 < \mu < 0$, two unbounded trajectories appear, intersecting the axes at the points $(v_K, 0)$ and $(v_L, 0)$ (see Figure 9b)
   For $b > 0$, the solution corresponding to a periodic orbit that intersects the horizontal axis at the points $(v_K, 0)$ and $(v_L, 0)$ is obtained from the integral

$$\int_{v}^{v_L} \frac{dv}{v\sqrt{(v - v_K)(v_L - v)}} = \pm\,|n-m|\sqrt{\frac{c}{m|n|p}}(\xi - \xi_0),$$

which leads to

$$v(\xi) = \frac{v_K v_L \sec^2(\varphi(\xi-\xi_0))}{v_K - v_L + v_L \sec^2(\varphi(\xi-\xi_0))},$$

where $\varphi = \frac{|n-m|}{2}\sqrt{\frac{c v_K v_L}{mnp}}$. The exact periodic wave solution of Eq. (2.6) is then given by

$$\psi(\xi) = \left(\frac{v_K v_L \sec^2(\varphi(\xi-\xi_0))}{v_K - v_L + v_L \sec^2(\varphi(\xi-\xi_0))}\right)^{\frac{1}{n-m}}. \tag{4.8}$$

In addition, the solution for the unbounded trajectory intersecting the axis at point $(v_L, 0)$ is expressed by the following integral:

$$\int_v^{\infty} \frac{dv}{v\sqrt{(v-v_K)(v-v_L)}} = \pm|n-m|\sqrt{\frac{c}{m|n|p}}(\xi-\xi_0),$$

where $v_K < 0 < v_L$. The solution is

$$v(\xi) = \frac{2v_K v_L}{v_K + v_L + (v_K - v_L)\cos[\varphi_1(\xi-\xi_0)]},$$

with the constant where $\varphi_1 = |n-m|\sqrt{\frac{-v_K v_L c}{m|n|p}}$. Then the singular wave solution of Eq. (2.6) becomes

$$\psi(\xi) = \left(\frac{2v_K v_L}{v_K + v_L + (v_K - v_L)\cos[\varphi_1(\xi-\xi_0)]}\right)^{\frac{1}{n-m}}. \tag{4.9}$$

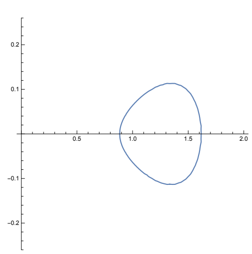

(a) $a > 0$, $c > 0$, $\overline{\Delta}_1 > 0$, $\mu > \mu_2$ or $\mu < \mu_1$

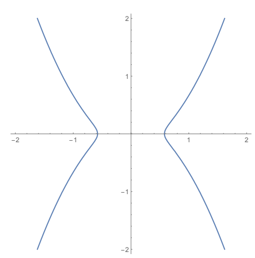

(b) $a > 0$, $c > 0$, $\overline{\Delta}_1 > 0$, $-1 < \mu < \mu_2$ or $\mu_1 < \mu < 0$

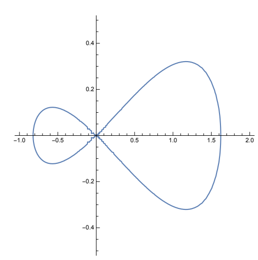

(c) $a < 0$, $c > 0$, $\overline{\Delta}_1 > 0$ $\mu > \mu_2$ or $\mu < \mu_1$

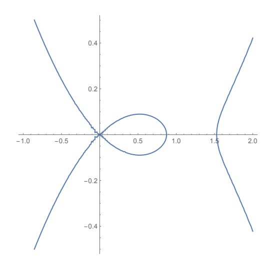

(d) $a < 0$, $c > 0$, $\overline{\Delta}_1 > 0$, $\mu_1 < \mu < \mu_2$

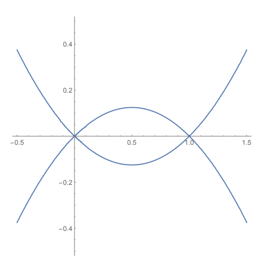

(e) $a < 0$, $c > 0$, $\overline{\Delta}_1 = 0$, $\mu = \mu_1$ or $\mu = \mu_2$

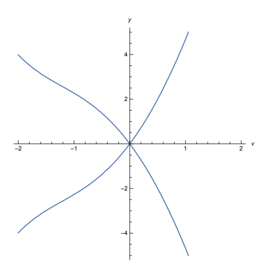

(f) $a < 0$, $c > 0$, $\overline{\Delta}_1 < 0$, $-1 < \mu < \mu_2$ or $\mu_1 < \mu < 0$

**Figure 9.** The level curves defined by Eq. (4.6) for $h = 0$, $p > 0$, $n = \frac{m(\mu+1)}{\mu}$.

2. When $a < 0$, $b > 0$, $c > 0$, and $\overline{\Delta}_1 > 0$, two homoclinic orbits occur for $\mu > \mu_2$ or $\mu < \mu_1$: One intersects the horizontal axis at $(v_L, 0)$ and approaches the origin $(0, 0)$, while the other departs from $(v_K, 0)$ and also approaches the origin (see Figure 9c). Furthermore, $\mu_1 < \mu < \mu_2$, a homoclinic orbit emerges that intersects the horizontal axis at $(v_K, 0)$ or $(v_L, 0)$ tends toward the origin (see Figure 9d). When $\overline{\Delta}_1 = 0$ and $\mu = \mu_1$ or $\mu = \mu_2$, a heteroclinic orbit occurs, intersecting the axis at $(v_2, 0)$ and approaching the origin (see Figure 9e). If $\overline{\Delta}_1 < 0$, four unbounded trajectories that approach the origin arise in the intervals $-1 < \mu < \mu_2$ or $\mu_1 < \mu < 0$ (see Figure 9f).
For the first homoclinic orbit intersecting the point $(v_K, 0)$ and approaching the origin, if $v_K < 0 < v_L$, the solution is obtained from the relation
$$\int_v^{v_L} \frac{dv}{v\sqrt{(v_L - v)(v - v_K)}} = |n - m| \sqrt{\frac{c}{m|n|p}}(\xi - \xi_0),$$
and is given by
$$v(\xi) = \frac{2v_K v_L}{v_K + v_L + (v_K - v_L)\cosh\left[\varphi_1(\xi - \xi_0)\right]}.$$
The corresponding exact bright solitary wave solution of Eq. (2.6) is
$$\psi(\xi) = \left(\frac{2v_K v_L}{v_K + v_L + (v_K - v_L)\cosh\left[\varphi_1(\xi - \xi_0)\right]}\right)^{\frac{1}{n-m}}. \tag{4.10}$$
Secondly, for the second homoclinic orbit that intersects the point $(v_K, 0)$ and approaches the origin, in the range $0 < v_K < v_L$, the solution is obtained from the following relation:
$$\int_v^{v_K} \frac{dv}{v\sqrt{(v_L - v)(v_K - v)}} = \pm\,|n - m| \sqrt{\frac{c}{m|n|p}}(\xi - \xi_0).$$
Solving this leads to the explicit form:
$$v(\xi) = \frac{v_K v_L \mathrm{sech}^2(\varphi_2(\xi - \xi_0))}{v_L - v_K \tanh^2(\varphi_2(\xi - \xi_0))},$$
where $\varphi_2 = |n - m|\sqrt{\frac{v_K v_L c}{4m|n|p}}$. Consequently, the bright solitary wave solution to Eq. (2.6) is given by:
$$\psi(\xi) = \left(\frac{v_K v_L \mathrm{sech}^2(\varphi_2(\xi - \xi_0))}{v_L - v_K \tanh^2(\varphi_2(\xi - \xi_0))}\right)^{\frac{1}{n-m}}. \tag{4.11}$$
Finally, for the heteroclinic orbit, the solution is obtained from
$$\int_{\frac{v_1}{2}}^{v} \frac{dv}{v(v_L - v)} = \pm\,|n - m| \sqrt{\frac{c}{m|n|p}}(\xi - \xi_0),$$
which yields the solution
$$v(\xi) = \pm v_L\left(1 - \frac{1}{1 + e^{\varphi_3(\xi - \xi_0)}}\right) = \pm\frac{v_L}{2}\left(1 + \tanh\left(\varphi_3(\xi - \xi_0)\right)\right),$$
where $v_L = v_2$ and $\varphi_3 = \frac{v_L|n-m|}{2}\sqrt{\frac{v_K v_L c}{4m|n|p}}$. Then, the exact kink (or anti-kink) wave solution of Eq. (2.6) becomes
$$\psi(\xi) = \left(\pm\frac{v_L}{2}\left(1 + \tanh\left(\varphi_3(\xi - \xi_0)\right)\right)\right)^{\frac{1}{n-m}}. \tag{4.12}$$

3. Let $a < 0$, $b < 0$, $c > 0$, and $\Delta_1 > 0$. If $\mu > \mu_2$ or $\mu < \mu_1$, the system admits a separatrix consisting of two homoclinic orbits (see Figure 9c). When $\mu_1 < \mu < \mu_2$, only one homoclinic orbit approaches the origin (see Figure 9d). Furthermore, for $\overline{\Delta}_1 = 0$, and $\mu = \mu_1$ or $\mu = \mu_2$, heteroclinic orbits emerge, connecting the equilibrium point to the origin (see Figure 9e). Finally, for $\overline{\Delta}_1 < 0$, unbounded orbits that approach the origin asymptotically exist when $-1 < \mu < \mu_2$ or $\mu_1 < \mu < 0$ (see Figure 9f).

**Remark 4.1.** For $h = 0$ and $c < 0$, the system of (4.5) exhibits similar structures as illustrated in Figure 9.

### 4.2. The exact traveling wave solutions of Eq. (2.6) given by the level curves $H(v, y) \neq 0$

In this section, we derive the exact traveling wave solution of (2.6) when $h \neq 0$.

1. By substituting $n = 3m$ into Eq. (4.4) and assuming $p > 0$, Eq. (4.4) can be rewritten as:

$$y^2 = \begin{cases} \dfrac{-4c}{3p}\left(\dfrac{-3h}{c}v + \dfrac{3a}{c}v^2 - \dfrac{3b}{2c}v^3 + v^4\right), & c < 0, \\ \dfrac{4c}{3p}\left(\dfrac{3h}{c}v - \dfrac{3a}{c}v^2 + \dfrac{3b}{2c}v^3 - v^4\right), & c > 0. \end{cases} \tag{4.13}$$

By substituting the square root of Eq. (4.13) into the first equation of system (4.3) and integrating the result over the interval $(v_j, v)$, one obtains

$$\int_{v_j}^{v} \frac{dv}{\sqrt{\eta_1 v\left(\frac{-3h}{c} + \frac{3a}{c}v - \frac{3b}{2c}v^2 + v^3\right)}} = \pm 2\sqrt{\frac{|c|}{3p}}(\xi - \xi_0), \tag{4.14}$$

where $\eta_1 = -sgn(c)$. Let the real zeros of the function

$$g_1(v) = -\frac{3h}{c}v + \frac{3a}{c}v^2 - \frac{3b}{2c}v^3 + v^4,$$

be denoted by $0, v_K, v_L$, and $v_M$. For the level curves of $H(v, y) = h$ defined by (4.4), the corresponding values at equilibrium points $H(v_i, 0) = h_i$ are computed as:

$$H(v_i, 0) = v_i(a - \frac{b}{2}v_i + \frac{c}{3}v_i^2) = h_i. \tag{4.15}$$

The solutions obtained from the bifurcation analysis for the case $\Delta_1 \geq 0$ are listed below in order.

(a) If $a > 0$, $b > 0$ and $c > 0$, then $0 < v_1 < v_2$. In this case, the equilibrium point $E_1(v_1, 0)$ is a saddle and $E_2(v_2, 0)$ is a center.

- For $0 < h_2 < h_1 = h$, the level curves $H(v, y) = h$ form two homoclinc orbits: The first homoclinic orbit that intersects the horizontal axis at $(v_M, 0)$ and approaches $E_1(v_1, 0)$ and the second homoclinic orbit intersecting the axis from $E_1(v_1, 0)$ to the point origin $O(0, 0)$, as shown in Figures 7a and 10a. Taking the first homoclinic orbit as the integration path, Eq. (4.14) becomes

$$\int_{v}^{v_M} \frac{dv}{(v - v_1)\sqrt{(v_M - v)v}} = \pm 2\sqrt{\frac{c}{3p}}(\xi - \xi_0),$$

where $0 < v_1 < v_M < v_2$. From this relation, we obtain the following parametric representation of the solitary wave solution:

$$v(\xi) = \frac{v_1 v_M}{v_1 + (v_M - v_1)\tanh^2(\varphi_1(\xi - \xi_0))},$$

where $\varphi_1 = \sqrt{\frac{v_1(v_M - v_1)c}{3p}}$. Then, the exact bright solitary wave solution of Eq. (2.6) is given by

$$\psi(\xi) = \left(\frac{v_1 v_M}{v_1 + (v_M - v_1)\tanh^2(\varphi_1(\xi - \xi_0))}\right)^{\frac{1}{2m}}. \tag{4.16}$$

For the second homoclinic orbit, Eq. (4.14) becomes

$$\int_0^v \frac{dv}{(v_1 - v)\sqrt{(v_M - v)v}} = \pm 2\sqrt{\frac{c}{3p}}(\xi - \xi_0).$$

It gives us that

$$v(\xi) = v_1 - \frac{v_M(v_M - v_1)}{v_M - v_1 + v_1 \tanh^2(\varphi_1(\xi - \xi_0))},$$

and the corresponding exact dark solitary wave solution of Eq. (2.6) is given by

$$\psi(\xi) = \left(v_1 - \frac{v_M(v_M - v_1)}{v_M - v_1 + v_1 \tanh^2(\varphi_1(\xi - \xi_0))}\right)^{\frac{1}{2m}}. \tag{4.17}$$

- For $0 < h_2 < h < h_1$, the level curves $H(v, y) = h$ admit two distinct orbits. The first is a periodic orbit, intersecting the $v$-axis at $(v_L, 0)$ and $(v_M, 0)$ and enclosing the equilibrium $(v_K, 0)$. The second is a closed trajectory that crosses the $v$-axis at $(v_K, 0)$ and approaches the origin asymptotically, as shown in Figures 7a and 10b. Choosing periodic orbit as the integration path, Eq. (4.14) becomes

$$\int_{v_L}^v \frac{dv}{\sqrt{v(v - v_K)(v - v_L)(v_M - v)}} = \pm 2\sqrt{\frac{c}{3p}}(\xi - \xi_0),$$

where $0 < v_K < v_L < v_2 < v_M$. From this, the periodic wave solutions is given by

$$v(\xi) = \frac{v_L(v_M - v_K) - v_K(v_M - v_L)\,\mathrm{sn}^2(\varphi_2(\xi - \xi_0), r_1)}{v_M - v_K - (v_M - v_L)\,\mathrm{sn}^2(\varphi_2(\xi - \xi_0), r_1)},$$

where $\varphi_2 = \sqrt{\frac{c v_L(v_M - v_K)}{3p}}$ and $r_1 = \sqrt{\frac{v_K(v_M - v_L)}{v_L(v_M - v_K)}}$. Thus, the exact periodic wave solution of Eq. (2.6) is given by

$$\psi(\xi) = \left(\frac{v_L(v_M - v_K) - v_K(v_M - v_L)\,\mathrm{sn}^2(\varphi_2(\xi - \xi_0), r_1)}{v_M - v_K - (v_M - v_L)\,\mathrm{sn}^2(\varphi_2(\xi - \xi_0), r_1)}\right)^{\frac{1}{2m}}. \tag{4.18}$$

On the other hand, taking the closed trajectories as the integration path, Eq. (4.14) becomes

$$\int_0^v \frac{dv}{\sqrt{v(v_K - v)(v_L - v)(v_M - v)}} = \pm 2\sqrt{\frac{c}{3p}}(\xi - \xi_0),$$

which gives us the following solution:

$$v(\xi) = \frac{v_K v_M \operatorname{sn}^2(\varphi_2(\xi-\xi_0), r_1)}{v_M - v_K \operatorname{cn}^2(\varphi_2(\xi-\xi_0), r_1)}.$$

Hence, the exact periodic wave solution of Eq. (2.6) is given by

$$\psi(\xi) = \left(\frac{v_K v_M \operatorname{sn}^2(\varphi_2(\xi-\xi_0), r_1)}{v_M - v_K \operatorname{cn}^2(\varphi_2(\xi-\xi_0), r_1)}\right)^{\frac{1}{2m}}. \tag{4.19}$$

- For $0 < h_2 < h_1 < h$, the level curves defined by $H(v, y) = h$ admit a periodic orbit that intersects the $v$-axis at the point $(v_M, 0)$ and approaches the origin $O(0,0)$, as shown in Figures 7a and 10c. If $0 < v_1 < v_2 < v_M$, then one obtains

$$\int_0^v \frac{dv}{\sqrt{v(v_M - v)[(v-b_1)^2 + a_1^2]}} = \pm 2\sqrt{\frac{c}{3p}}(\xi - \xi_0).$$

This gives us the following solution:

$$v(\xi) = \frac{v_M B(1 - \operatorname{cn}(\varphi_3(\xi-\xi_0), r_2))}{A + B + (A-B)\operatorname{cn}(\varphi_3(\xi-\xi_0), r_2)},$$

where $\varphi_3 = 2\sqrt{\frac{cAB}{3p}}$, $r_2 = \sqrt{\frac{v_M^2 - (A-B)^2}{4AB}}$, $A^2 = (v_M - b_1)^2 + a_1^2$, $B^2 = b_1^2 + a_1^2$. Thus, we obtain the exact periodic wave solution of Eq. (2.6) given by

$$\psi(\xi) = \left(\frac{v_M B(1 - \operatorname{cn}(\varphi_3(\xi-\xi_0), r_2))}{A + B + (A-B)\operatorname{cn}(\varphi_3(\xi-\xi_0), r_2)}\right)^{\frac{1}{2m}}. \tag{4.20}$$

(b) For $a < 0$, $b < 0$ and $c > 0$, we have $v_1 < 0 < v_2$. In this case, both $E_1(v_1, 0)$ and $E_2(v_2, 0)$ are centers.

- For $h_2 < h = 0 < h_1$, from (4.15), the level curves $H(v, y) = h$ (see Figures 7d and 10d) generate two homoclinic orbits: One intersects the horizontal axis at $(v_L, 0)$ and approaches the origin $(0, 0)$; the other departs from $(v_K, 0)$ and also approaches the origin.

Corresponding to this homoclinic orbit (intersecting $(v_L, 0)$), the solution $v = v(\xi)$ obtained from (4.14), assuming $v_K < v_1 < 0 < v_2 < v_L$, satisfies the integral equation

$$\int_v^{v_L} \frac{dv}{v\sqrt{(v_L - v)(v - v_K)}} = \pm 2\sqrt{\frac{c}{3p}}(\xi - \xi_0).$$

From this, with the coefficient

$$\varphi_4 = \sqrt{\frac{-c v_K v_L}{3p}},$$

the solution is given by

$$v(\xi) = \frac{v_K v_L \operatorname{sech}^2(\varphi_4(\xi-\xi_0))}{v_K - v_L \tanh^2(\varphi_4(\xi-\xi_0))}.$$

Therefore, the exact bright solitary wave solution of Eq. (2.6) becomes

$$\psi(\xi) = \left(\frac{v_K v_L \operatorname{sech}^2(\varphi_4(\xi-\xi_0))}{v_K - v_L \tanh^2(\varphi_4(\xi-\xi_0))}\right)^{\frac{1}{2m}}. \tag{4.21}$$

- For $h_2 < h < 0 < h_1$, Eq. (4.15), the level curves $H(v, y) = h$ (see Figures 7d and 10e) form a closed orbit intersecting the horizontal axis at $(v_K, 0)$ and passing through the origin $(0, 0)$, together with a periodic orbit centered at $E_2(v_2, 0)$, which intersects the axis at $(v_L, 0)$ and $(v_M, 0)$.
  Corresponding to the periodic orbit centered at $E_2(v_2, 0)$, the solution $v = v(\xi)$ of (4.14), for $v_K < 0 < v_L < v_2 < v_M$, satisfies

$$\int_{v_L}^{v} \frac{dv}{\sqrt{(v_M - v)(v_L - v)v(v - v_K)}} = \pm 2\sqrt{\frac{c}{3p}}(\xi - \xi_0).$$

Using the coefficients

$$\varphi_5 = \sqrt{\frac{cv_M(v_L - v_K)}{3p}}, \qquad r_3 = \sqrt{\frac{v_K(v_L - v_M)}{v_M(v_L - v_K)}}$$

the solution becomes

$$v(\xi) = \frac{v_M v_L}{v_M - (v_M - v_L)\,\mathrm{sn}^2(\varphi_5(\xi - \xi_0))}.$$

Thus, the exact periodic wave solution of Eq. (2.6) is given by

$$\psi(\xi) = \left(\frac{v_M v_L}{v_M - (v_M - v_L)\,\mathrm{sn}^2(\varphi_5(\xi - \xi_0))}\right)^{\frac{1}{2m}}. \tag{4.22}$$

(c) For $a > 0$, $b < 0$ and $c < 0$, we have $v_2 < 0 < v_1$. In this case, both equilibrium points $E_1(v_1, 0)$ and $E_2(v_2, 0)$ are saddles.

- For $h_2 < 0 < h_1 = h$, from (4.15), the level curves $H(v, y) = h$ (see Figures 7e and 10f) form a homoclinic orbit that intersects the horizontal axis at the saddle point $E_1(v_1, 0)$ and approaches the origin. For the homoclinic orbit corresponding to this curve, the solution $v = v(\xi)$ obtained from (4.14), where the intersection point $(v_K, 0)$ of the curve with the horizontal axis satisfies $v_K < 0 < v_1$, is derived from the integral

$$\int_{0}^{v} \frac{dv}{(v_1 - v)\sqrt{v(v - v_K)}} = 2\sqrt{\frac{-c}{3p}}(\xi - \xi_0).$$

Using the coefficient

$$\varphi_6 = 2\sqrt{\frac{-cv_1(v_1 - v_K)}{3p}},$$

the solution becomes

$$v(\xi) = v_1 + \frac{2v_1(v_1 - v_K)}{v_K - 2v_1 + v_K\cosh(\varphi_6(\xi - \xi_0))}.$$

Thus, the exact dark solitary wave solution of Eq. (2.6) is given by

$$\psi(\xi) = \left(v_1 + \frac{2v_1(v_1 - v_K)}{v_K - 2v_1 + v_K\cosh(\varphi_6(\xi - \xi_0))}\right)^{\frac{1}{2m}}. \tag{4.23}$$

- For $h_2 < 0 < h < h_1$, from (4.15), the level curves $H(v, y) = h$ (see Figures 7e and 10g) form a periodic orbit that intersects the horizontal axis at $(v_L, 0)$ and approaches the origin.
  The periodic solution $v = v(\xi)$ corresponding to this orbit, obtained from (4.14), with the points $(v_K, 0)$, $(v_L, 0)$, and $(v_M, 0)$ satisfying $v_K < 0 < v_L < v_M$, is derived from the integral

$$\int_0^v \frac{dv}{\sqrt{(v-v_K)v(v_L-v)(v_M-v)}} = \pm 2\sqrt{\frac{-c}{3p}}(\xi-\xi_0).$$

  Using the coefficients

$$\varphi_7 = \sqrt{\frac{-cv_M(v_L-v_K)}{3p}}, \qquad r_4 = \sqrt{\frac{v_L(v_M-v_K)}{v_M(v_L-v_K)}},$$

  the solution becomes

$$v(\xi) = \frac{v_K v_L \operatorname{sn}^2(\varphi_7(\xi-\xi_0), r_4)}{v_K - v_L \operatorname{cn}^2(\varphi_7(\xi-\xi_0), r_4)}.$$

  Therefore, the exact periodic wave solution of Eq. (2.6) is given by

$$\psi(\xi) = \left(\frac{v_K v_L \operatorname{sn}^2(\varphi_7(\xi-\xi_0), r_4)}{v_K - v_L \operatorname{cn}^2(\varphi_7(\xi-\xi_0), r_4)}\right)^{\frac{1}{2m}}. \tag{4.24}$$

(d) For $a < 0$, $b < 0$ and $c < 0$, we have $0 < v_2 < v_1$. In this case, the equilibrium point $E_1(v_1, 0)$ is a saddle, and $E_2(v_2, 0)$ is a center.

- For $h_2 = h < h_1 < 0$, from (4.15), the level curves $H(v, y) = h$ (see Figures 7f and 10h) form a homoclinic orbit that intersects the horizontal axis at $(v_L, 0)$ and tends to the point $E_1(v_1, 0)$.
  The solution $v = v(\xi)$ corresponding to this homoclinic orbit obtained from (4.14), where the horizontal axis intersection point $(v_L, 0)$ satisfies $0 < v_L < v_1$, is given by the integral

$$\int_{v_L}^v \frac{dv}{(v_1-v)\sqrt{(v-v_L)v}} = \pm 2\sqrt{\frac{-c}{3p}}(\xi-\xi_0).$$

  With the coefficient

$$\varphi_8 = 2\sqrt{\frac{-cv_1(v_1-v_L)}{3p}},$$

  the solution takes the form

$$v(\xi) = v_1 + \frac{2v_1(v_1-v_L)}{v_L - 2v_1 - v_L\cosh\big(\varphi_8(\xi-\xi_0)\big)}.$$

  Thus, the exact dark solitary wave solution of Eq. (2.6) is given by

$$\psi(\xi) = \left(v_1 + \frac{2v_1(v_1-v_L)}{v_L - 2v_1 - v_L\cosh\big(\varphi_8(\xi-\xi_0)\big)}\right)^{\frac{1}{2m}}. \tag{4.25}$$

- For $h_2 < h < h_1 < 0$, from (4.15), the level curves $H(v, y) = h$ (see Figures 7f and 10i) form a periodic orbit centered at $E_2(v_2, 0)$ intersecting the horizontal axis at the points $(v_L, 0)$ and $(v_M, 0)$.
  The corresponding periodic solution $v = v(\xi)$, derived from (4.14), is given by the integral

$$\int_{v}^{v_L} \frac{dv}{\sqrt{(v - v_K)v(v_L - v)(v_M - v)}} = \pm 2\sqrt{\frac{-c}{3p}}(\xi - \xi_0),$$

  where $0 < v_K < v_2 < v_L < v_M$. Using the coefficients

$$\varphi_9 = \sqrt{\frac{-cv_L(v_M - v_K)}{3p}}, \quad r_5 = \sqrt{\frac{v_M(v_L - v_K)}{v_L(v_M - v_K)}},$$

  the solution becomes

$$v(\xi) = \frac{v_M(v_L - v_K)\,\mathrm{sn}^2(\varphi_9(\xi - \xi_0), r_5) - v_L(v_M - v_K)}{(v_L - v_K)\,\mathrm{sn}^2(\varphi_9(\xi - \xi_0), r_5) - (v_M - v_K)}.$$

  Thus, the exact periodic wave solution Eq. (2.6) is given by

$$\psi(\xi) = \left(\frac{v_M(v_L - v_K)\,\mathrm{sn}^2(\varphi_9(\xi - \xi_0), r_5) - v_L(v_M - v_K)}{(v_L - v_K)\,\mathrm{sn}^2(\varphi_9(\xi - \xi_0), r_5) - (v_M - v_K)}\right)^{\frac{1}{2m}}. \tag{4.26}$$

- For $h < h_2 < h_1 < 0$, from (4.15), the level curve $H(v, y) = h$ (see Figures 7f and 10j) forms an unbounded orbit that intersects the horizontal axis at $(v_L, 0)$ and extending to infinity.
  The corresponding solution $v = v(\xi)$, derived from (4.14), is given by the integral

$$\int_{v_L}^{v} \frac{dv}{\sqrt{v(v - v_L)[(v - b_1)^2 + a_1^2]}} = \pm 2\sqrt{\frac{-c}{3p}}(\xi - \xi_0),$$

  where $0 < v_L$. With coefficients

$$\varphi_{10} = 2\sqrt{\frac{-cAB}{3p}}, \quad r_6 = \sqrt{\frac{(A + B)^2 - v_L^2}{4AB}},$$

  and

$$A^2 = (v_L - b_1)^2 + a_1^2, \quad B^2 = b_1^2 + a_1^2,$$

  the solution is

$$v(\xi) = \frac{v_L B\big(1 + \mathrm{cn}(\varphi_{10}(\xi - \xi_0), r_6)\big)}{B - A + (A + B)\mathrm{cn}(\varphi_{10}(\xi - \xi_0), r_6)}.$$

  Hence, the exact periodic wave solution of Eq. (2.6) is given by

$$\psi(\xi) = \left(\frac{v_L B\big(1 + \mathrm{cn}(\varphi_{10}(\xi - \xi_0), r_6)\big)}{B - A + (A + B)\mathrm{cn}(\varphi_{10}(\xi - \xi_0), r_6)}\right)^{\frac{1}{2m}}. \tag{4.27}$$

- For $h_2 < h_1 = h = 0$, the level curves defined by $H(v, y) = 0$, there exists two heteroclinic orbit passing through the origin and approaching the saddle point $(v_1, 0)$ (see Figure 7g and 10k). Choosing a heteroclinic orbit as the integral path, Eq. (4.14) becomes

$$\int_{v_1/2}^{v} \frac{dv}{v\,(v_1 - v)} = \pm 2\sqrt{\frac{-c}{3p}}(\xi - \xi_0),$$

where $0 < v_1$. From this, we obtain the parametric representation of a kink wave solution of system (4.5) given by

$$v\,(\xi) = \pm\frac{v_1}{2}\left(1 + \tanh(v_1\sqrt{\frac{-c}{3p}}(\xi - \xi_0))\right).$$

Thus, the exact kink wave solution of Eq. (2.6) is given by

$$v\,(x, t) = \left[\frac{v_1}{2}\left(1 + \tanh(v_1\sqrt{\frac{-c}{3p}}(\xi - \xi_0))\right)\right]^{\frac{1}{2m}}. \tag{4.28}$$

(e) If $\Delta_1 = 0$, $c > 0$, $a > 0$, and $b > 0$, then $v_1 > 0$, and the equilibrium point $E_1(v_1, 0)$ becomes a cusp. For $0 < h_1 = h$, the level curves $H(v, y) = h$, derived from Eq. (4.15) admit a trajectory that intersects the horizontal axis at $(v_1, 0)$ and tends to the origin, as shown in Figures 8a and 10l.
For the corresponding solution $v = v(\xi)$, using the identity

$$\int_0^v \frac{dv}{(v_1 - v)\sqrt{(v_1 - v)v}} = \pm 2\sqrt{\frac{c}{3p}}(\xi - \xi_0),$$

we obtain

$$v(\xi) = \frac{{v_1}^3 c(\xi - \xi_0)^2}{{v_1}^2 c(\xi - \xi_0)^2 + 3p}.$$

Then, the exact dark solitary wave solution of Eq. (2.6) becomes

$$\psi(\xi) = \left(\frac{{v_1}^3 c(\xi - \xi_0)^2}{{v_1}^2 c(\xi - \xi_0)^2 + 3p}\right)^{\frac{1}{2m}}. \tag{4.29}$$

(f) If $\Delta_1 = 0$, $c < 0$, $a < 0$, and $b < 0$, then $v_1 > 0$, and the equilibrium point $E_1(v_1, 0)$ becomes a cusp. For $h = h_1 < 0$, the level curves defined by $H(v, y) = h$ correspond to an orbit that intersects the $v$-axis at $(v_1, 0)$ and extends to infinity, forming a cusp orbit, as illustrated in Figures 8b and 10(m). The solutions associated with these curves, valid for $0 < v_1$, are obtained from the integral equation:

$$\int_v^{\infty} \frac{dv}{(v - v_1)\,\sqrt{v\,(v - v_1)}} = \pm 2\sqrt{\frac{-c}{3p}}\;(\xi - \xi_0).$$

This leads to a singular wave solution, with the coefficient $\varphi_{11} = v_1\sqrt{\frac{-c}{3p}}$, which is explicitly given by:

$$v(\xi) = \frac{v_1[1 \pm \varphi_{11}(\xi - \xi_0)]^2}{\varphi_{11}(\xi - \xi_0)[\varphi_{11}(\xi - \xi_0) \pm 2]}.$$

Then the exact singular wave solution of Eq. (2.6) becomes

$$\psi(\xi) = \left( \frac{v_1[1 \pm \varphi_{11}(\xi - \xi_0)]^2}{\varphi_{11}(\xi - \xi_0)[\varphi_{11}(\xi - \xi_0) \pm 2]} \right)^{\frac{1}{2m}}. \tag{4.30}$$

2. When $n = -m$, $b = 0$, and $p > 0$, the solutions of Eq. (2.6) are given based on the phase portraits of the system (4.5). In this case, Eq. (4.4) can be written as

$$y^2 = \begin{cases} \dfrac{-4c}{p}\left(\dfrac{a}{c}v^2 + \dfrac{h}{c}v^3 - v^4\right), & c > 0, \\ \dfrac{4c}{p}\left(-\dfrac{a}{c}v^2 - \dfrac{h}{c}v^3 + v^4\right), & c < 0. \end{cases} \tag{4.31}$$

Substituting Eq. (4.31) into $y = \frac{dv}{d\xi}$, the solutions $v = v(\xi)$ can be obtained on the interval $(v_j, v)$ from the equality

$$\int_{v_j}^{v} \frac{dv}{\sqrt{\eta_1 v^2 \left(\frac{a}{c} + \frac{h}{c}v - v^2\right)}} = \pm 2\sqrt{\frac{|c|}{p}}(\xi - \xi_0),$$

where $\eta_1 = -sgn(c)$.
Now we assume that 0, $v_L$, and $v_M$ are the roots of the function $g_2(v) = \frac{a}{c}v^2 + \frac{h}{c}v^3 - v^4$. From Eq. (4.4), the values of the level curves $H(v_i, 0) = h_i$ are obtained from

$$H(v_i, 0) = v_i^{-2}(-a + cv_i^2) = h_i. \tag{4.32}$$

(a) If $a < 0$ and $c > 0$, then $v_2 < 0 < v_1$. In this case, both equilibrium points $E_1(v_1, 0)$ and $E_2(v_2, 0)$ are saddle points.

- For $h_2 < 0 < h_1 = h$, from Eq. (4.32), the level curves $H(v, y) = h$ form heteroclinic orbits that intersect the horizontal axis at $(v_1, 0)$ and tend to the origin, as shown in Figures 8c and 10k. For the heteroclinic orbit corresponding to the solution $v = v(\xi)$, if we choose $v_2 < 0 < v_1$, then from the integral identity

$$\int_{\frac{v_1}{2}}^{v} \frac{dv}{v(v_M - v)} = \pm 2\sqrt{\frac{c}{p}}(\xi - \xi_0),$$

we obtain the solution

$$v(\xi) = \pm\frac{1}{2}v_L\left[1 + \tanh\left(v_L\sqrt{\frac{c}{p}}\,(\xi - \xi_0)\right)\right],$$

where $v_L = v_1$. The corresponding exact kink wave solution of Eq. (2.6) is given by

$$\psi(\xi) = \left(\frac{1}{2}v_L\left[1 + \tanh\left(v_L\sqrt{\frac{c}{p}}\,(\xi - \xi_0)\right)\right]\right)^{\frac{1}{2n}}. \tag{4.33}$$

- For $h_2 < 0 < h_1 = h$, from Eq. (4.32), H(v,y)=0 level curves intersect the horizontal axis at the point $(v_L, 0)$ and define a homoclinic orbit that tends to converges at the origin, as illustrated in Figures 8c and 10n. The solution $v = v(\xi)$ corresponding to this orbit is obtained from

$$\int_{v}^{v_L} \frac{dv}{v\sqrt{(v_L - v)(v_M - v)}} = \pm 2\sqrt{\frac{c}{p}}(\xi - \xi_0).$$

This gives us the following solution:

$$v(\xi) = \frac{v_L v_M \operatorname{sech}^2(\varphi_{12}(\xi - \xi_0))}{v_M - v_L \tanh^2(\varphi_{12}(\xi - \xi_0))},$$

where $0 < v_L < v_M < v_1$ and $\varphi_{12} = \sqrt{\frac{c\ v_L v_M}{p}}$. The corresponding bright solitary wave solution of Eq. (2.6) is given by

$$\psi(\xi) = \left(\frac{v_L v_M \operatorname{sech}^2(\varphi_{12}(\xi - \xi_0))}{v_M - v_L \tanh^2(\varphi_{12}(\xi - \xi_0))}\right)^{\frac{1}{2n}}. \tag{4.34}$$

(b) If $a < 0$ and $c < 0$, then $v_2 < 0 < v_1$. In this case, both equilibrium points $E_1(v_1, 0)$ and $E_2(v_2, 0)$ are centers.

- For $h < h_1 < 0 < h_2$, the level curves $H(v, y) = h$, obtained from Eq. (4.32), form periodic orbits centered at $E_1(v_1, 0)$ that intersect the horizontal axis at $(v_L, 0)$ and $(v_M, 0)$, as shown in Figures 8d and 10o.
  For the solution $v = v(\xi)$ corresponding to these periodic orbits, if $0 < v_L < v_1 < v_M$, then from the integral identity

$$\int_{v_L}^{v} \frac{dv}{v\sqrt{(v_M - v)(v - v_L)}} = \pm 2\sqrt{\frac{-c}{p}}(\xi - \xi_0),$$

we obtain the solution

$$v(\xi) = \frac{v_L v_M \sec^2(\varphi_{13}(\xi - \xi_0))}{v_M + v_L \tan^2(\varphi_{13}(\xi - \xi_0))},$$

where $\varphi_{13} = \sqrt{\frac{-c\ v_L v_M}{p}}$. The corresponding periodic wave solutions of Eq. (2.6) is given by

$$\psi(\xi) = \left(\frac{v_L v_M \sec^2(\varphi_{13}(\xi - \xi_0))}{v_M + v_L \tan^2(\varphi_{13}(\xi - \xi_0))}\right)^{\frac{1}{2n}}. \tag{4.35}$$

## 5. Graphical representation

In this section, we present two-dimensional (2D), three-dimensional (3D), and contour plot representations of some representative wave structures, including singular periodic, bright solitary, dark solitary, and kink-type solutions, in order to analyze the influence of the fractional orders $\beta_1$ and $\beta_2$ on the wave dynamics. In each graphical illustration, the parameters are chosen to satisfy the definitions and constraints imposed by the equation.

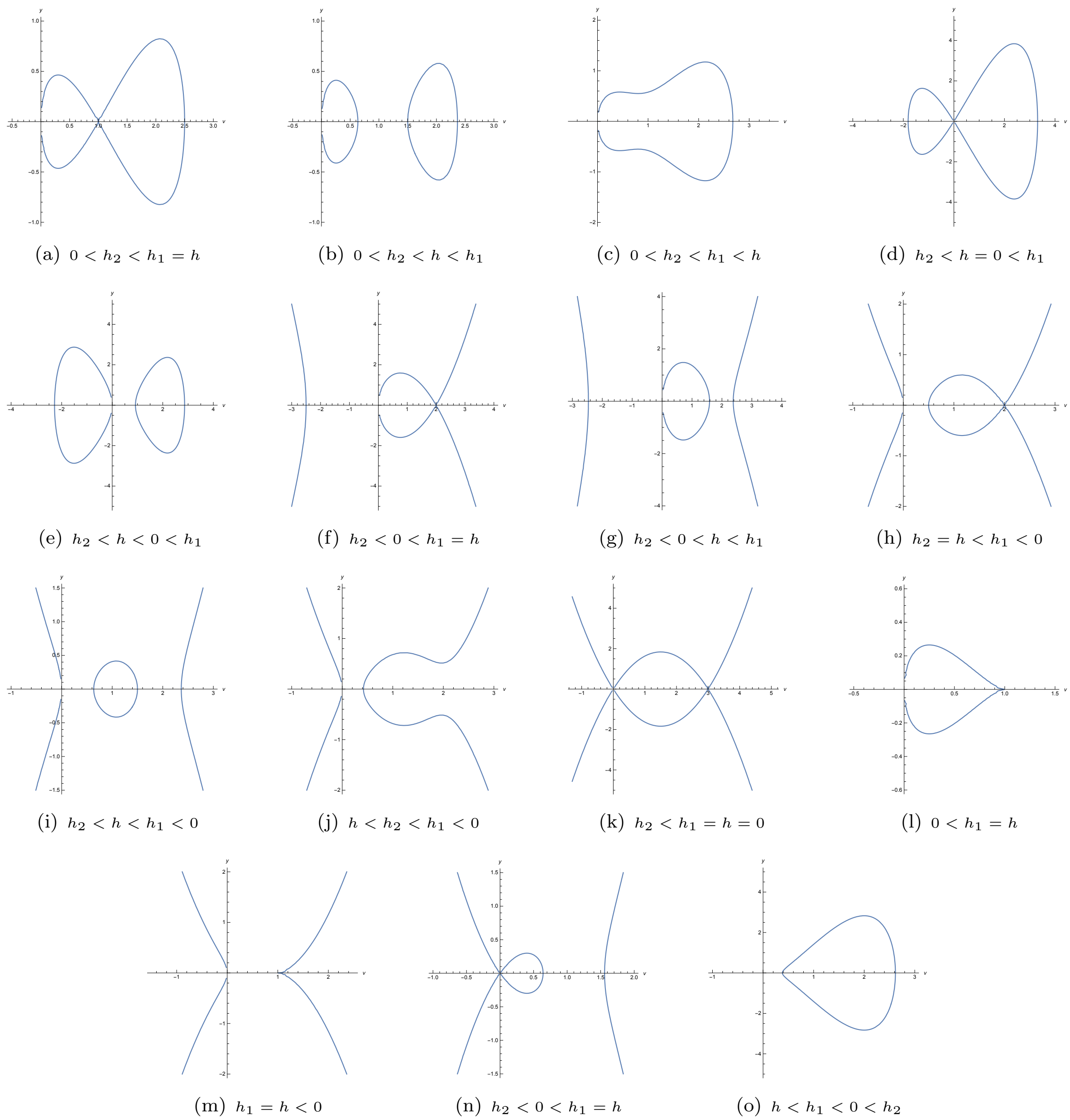

(a) $0 < h_2 < h_1 = h$ (b) $0 < h_2 < h < h_1$ (c) $0 < h_2 < h_1 < h$ (d) $h_2 < h = 0 < h_1$

(e) $h_2 < h < 0 < h_1$ (f) $h_2 < 0 < h_1 = h$ (g) $h_2 < 0 < h < h_1$ (h) $h_2 = h < h_1 < 0$

(i) $h_2 < h < h_1 < 0$ (j) $h < h_2 < h_1 < 0$ (k) $h_2 < h_1 = h = 0$ (l) $0 < h_1 = h$

(m) $h_1 = h < 0$ (n) $h_2 < 0 < h_1 = h$ (o) $h < h_1 < 0 < h_2$

**Figure 10.** The level curves defined by Eqs. (4.13) and (4.31) for $h \neq 0$.

- The application of transformation (2.4) to Eq. (3.8) yields the following explicit solution to Eq. (2.2):

$$q(x,t) = \left(\frac{v_L v_K sn^2(\Omega_1(\lambda(t+\frac{1}{\Gamma(\beta_1)})^{\beta_1} + \alpha(x+\frac{1}{\Gamma(\beta_2)})^{\beta_2} - \xi_0),\ m_1)}{v_K - v_L + v_L sn^2(\Omega_1(\lambda(t+\frac{1}{\Gamma(\beta_1)})^{\beta_1} + \alpha(x+\frac{1}{\Gamma(\beta_2)})^{\beta_2} - \xi_0),\ m_1)}\right)^{\frac{1}{n}}. \quad (5.1)$$

Eq. (5.1) is a periodic wave solution with singularities for Eq. (2.2), corresponding to a family of closed orbits that contact the singular line $v = 0$ at the origin $O(0,0)$, as illustrated in Figure 1a. Figures 11a–c present the 3D and contour representations of Eq. (5.1) for various values of $\beta_1$ ($\beta_1$=1,0.8,0.65), while Figure 11d illustrates the corresponding 2D profile. Figure 11d shows that as the fractional temporal order $\beta_1$ decreases while keeping $\beta_2 = 1$, the solution $q(0,t)$ exhibits a temporal delay and an increase in the temporal period, whereas Figures 12a–d show that decreasing $\beta_2$ leads to a broader spatial distribution and longer spatial periods. These graphical results reveal that the beta fractional orders play an important role in controlling the temporal and spatial behavior of the wave profiles.

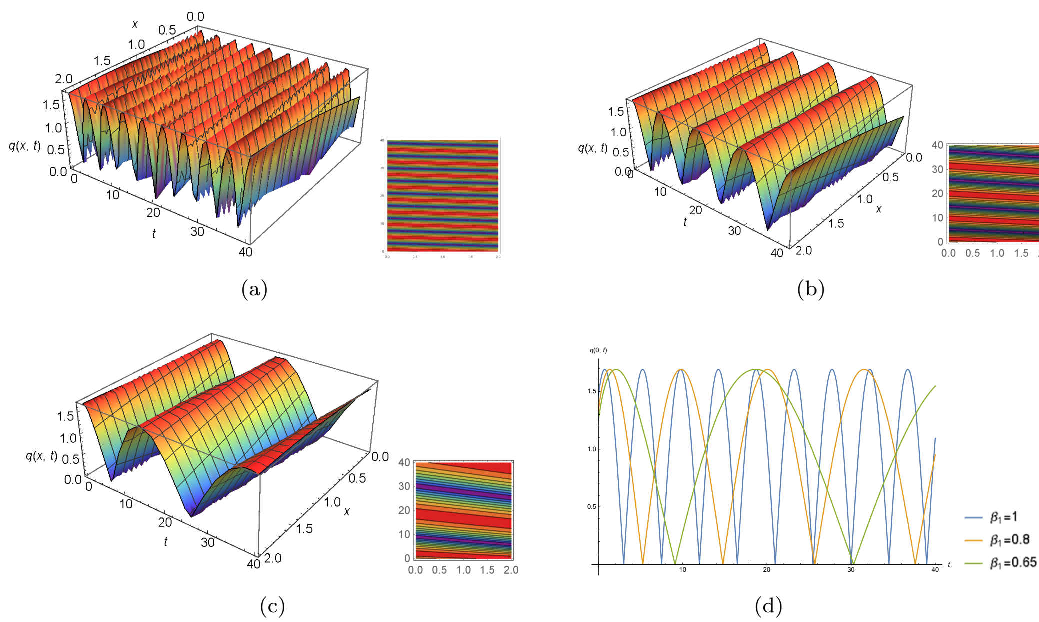


**Figure 11.** Graphical representations of the periodic wave solution with singularities given in Eq. (5.1) with parameters $\alpha = a = c = k = 1$, $b = 6$, $\lambda = 2$, $n = 2$, $m = 3$, $\xi_0 = 0$ and $\beta_2 = 1$. (a)–(c) $3D$ and contour plots of the solution for $\beta_1 = 1$, 0.8, and 0.65, respectively, (d) $2D$ representations across various values of $\beta_1$.

- By applying transformation (2.4) to Eq. (3.21), the solution of Eq. (2.2), as given below, is obtained.

$$q(x,t) = \left( \frac{v_2 v_L}{v_L + (v_2 - v_L) sech^2(\omega_4(\lambda(t + \frac{1}{\Gamma(\beta_1)})^{\beta_1} + \alpha(x + \frac{1}{\Gamma(\beta_2)})^{\beta_2} - \xi_0)} \right)^{\frac{1}{n}}. \tag{5.2}$$

The solution (5.2) is a solitary wave solution of Eq. (2.2), corresponding to a homoclinic orbit, as illustrated in Figure 1c. The 3D and contour representations of this solution are presented in Figures 13a–d for various values of $\beta_1$ ($\beta_1$=1,0.8,0.6). The results presented in Figure 13d illustrate the influence of the temporal fractional order $\beta_1$ on the wave $q(x,3)$ profile, with the spatial order fixed at $\beta_2 = 1$. The corresponding wave solutions exhibit bright solitary wave profiles for all values of $\beta_1$. As $\beta_1$ decreases from 1.0 to lower values (e.g., 0.8 and 0.6), the solitary wave profile shifts toward earlier spatial positions while preserving its bright solitary wave structure. These results show that the temporal fractional order $\beta_1$ affects the propagation behavior of the solitary wave solutions.

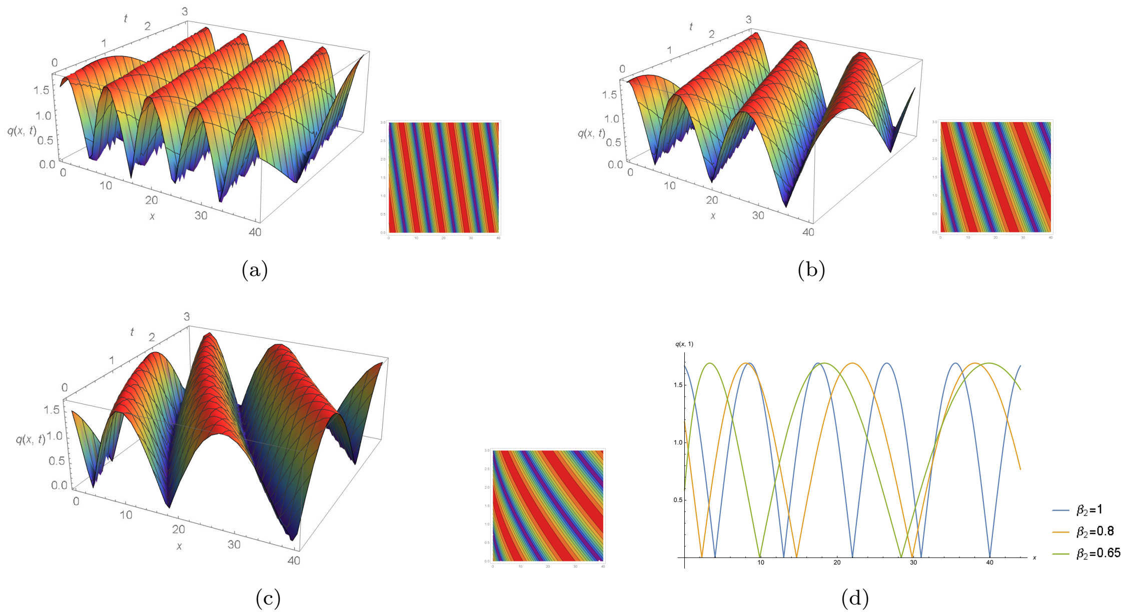


**Figure 12.** Graphical representations of the periodic wave solution with singularities given in Eq. (5.1) with parameters $\alpha = a = c = k = 1$, $b = 6$, $\lambda = 2$, $n = 2$, $m = 3$, $\xi_0 = 0$ and $\beta_1 = 1$. (a)–(c) $3D$ and contour plots of the solution for $\beta_2 = 1$, 0.8, and 0.65, respectively, (d) $2D$ representations across various values of $\beta_2$.

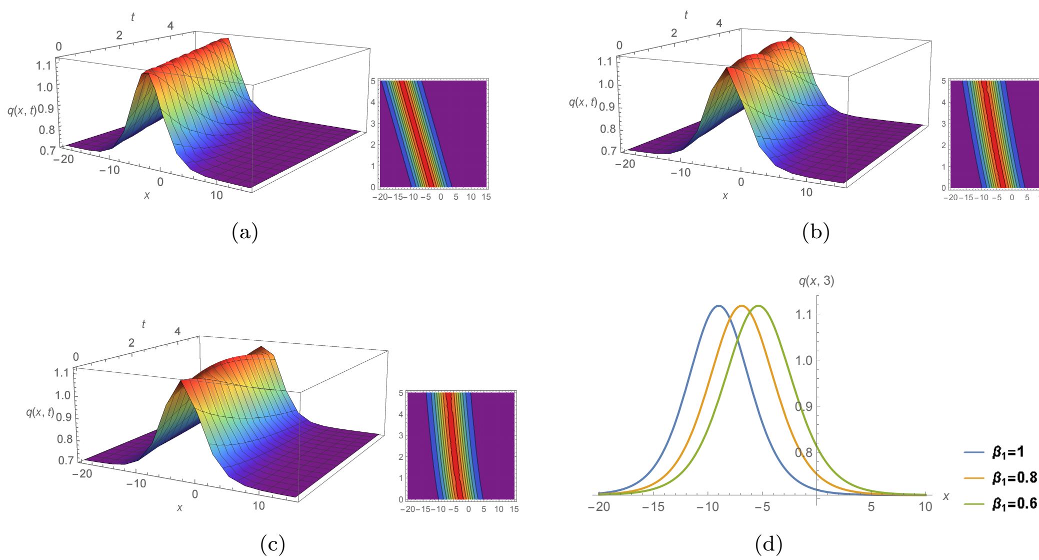


**Figure 13.** Graphical representations of the solitary wave solution given in (5.2) with parameters $\alpha = c = k = 1$, $a = -3$, $b = -2$, $\lambda = 2$, $n = -2$, $m = 2$, $\xi_0 = 0$ and $\beta_2 = 1$. (a)–(c) $3D$ and contour plots of the solution for $\beta_1 = 1$, 0.8, and 0.6, respectively, (d) $2D$ representations across various values of $\beta_1$.

- The application of the transformation (2.4) to Eq. (4.18) yields the following solution of Eq. (2.3):

$$q(x,t)=\Big(\frac{v_L(v_M-v_K)-v_K(v_M-v_L)sn^2(\varphi_2(\lambda(t+\frac{1}{\Gamma(\beta_1)})^{\beta_1}+\alpha(x+\frac{1}{\Gamma(\beta_2)})^{\beta_2}-\xi_0),\ r_1)}{v_M-v_K-(v_M-v_L)sn^2(\varphi_2(\lambda(t+\frac{1}{\Gamma(\beta_1)})^{\beta_1}+\alpha(x+\frac{1}{\Gamma(\beta_2)})^{\beta_2}-\xi_0),\ r_1)}\Big)^{\frac{1}{2m}}. \tag{5.3}$$

The influence of the fractional derivative order $\beta$ on the emergence of periodic wave solutions is illustrated in Figure 14. The solution given in Eq. (5.3) represents a periodic

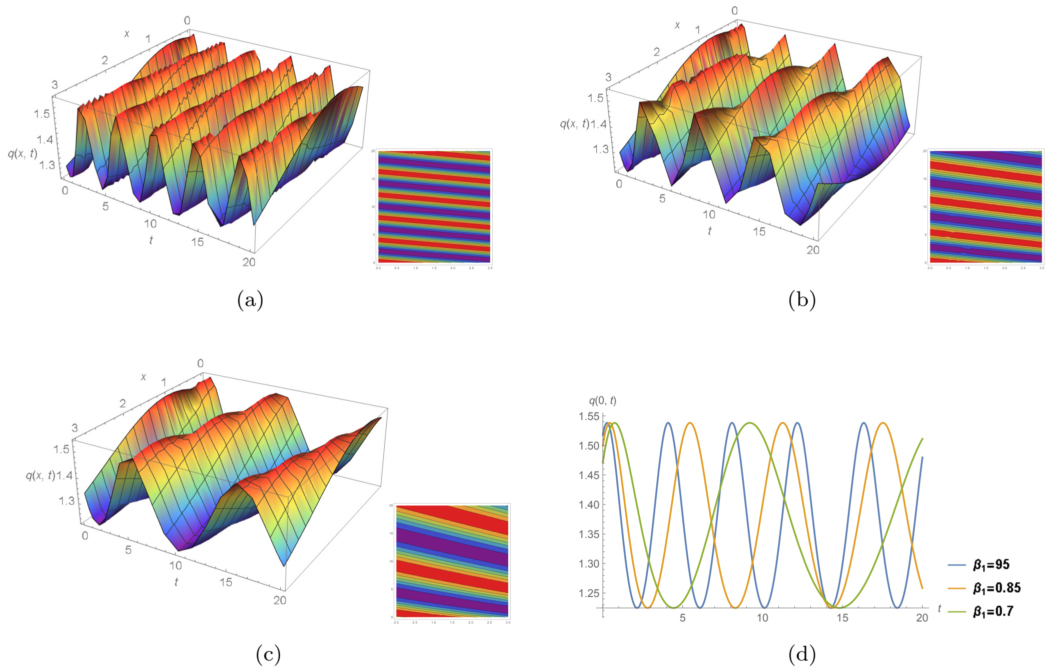


**Figure 14.** Graphical representations of the periodic wave solution given in (5.3) with parameters $\alpha = m = c = k = 1$, $a = 2$, $b = 3$, $\lambda = 2$, $n = 3$, $\xi_0 = 0$ and $\beta_2 = 1$. (a)–(c) $3D$ and contour plots of the solution for $\beta_1 = 0.95$, 0.85, and 0.7, respectively, (d) $2D$ representations across various values of $\beta_1$.

wave profile corresponding to a family of periodic orbits, as illustrated in Figure 9b. Figures 14a-c present the 3D and contour representations of this solution for various values of the fractional orders ($\beta_2 = 1, \beta_1 = 0.95, 0.85, 0.7$), while Figure 14d depicts the associated 2D wave profiles. As shown in 14d, although the amplitude of the solution remains essentially unaffected by changes in the fractional order, the wave exhibits a temporal delay in its peak response and a longer oscillation period with decreasing $\beta_1$. These results show the influence of the fractional temporal order on the behavior of the periodic wave solutions.

- Applying the transformation (2.4) to Eq. (4.25) yields the following solution of Eq. (2.3):

$$q(x,t)=\Big(v_1+\frac{2v_1(v_1-v_L)}{v_L-2v_1-v_L\cosh(\varphi_8(\lambda(t+\frac{1}{\Gamma(\beta_1)})^{\beta_1}+\alpha(x+\frac{1}{\Gamma(\beta_2)})^{\beta_2}-\xi_0)}\Big)^{\frac{1}{2m}}. \tag{5.4}$$

Figures 15a–c depict the dark soliton profiles of Eq. (5.4) for $\alpha = m = k = 1$, $a = -2$, $b = -3$, $c = -1$ $\lambda = 2$, $n = 3$, and $\beta_2 = 1$. Figure 15d describes the effect of different values of $\beta_1$ on the solution profiles. From this figure, we observe that as $\beta_1$ decreases, the dark soliton profile shifts rightward at fixed $t$ while preserving its overall wave structure.

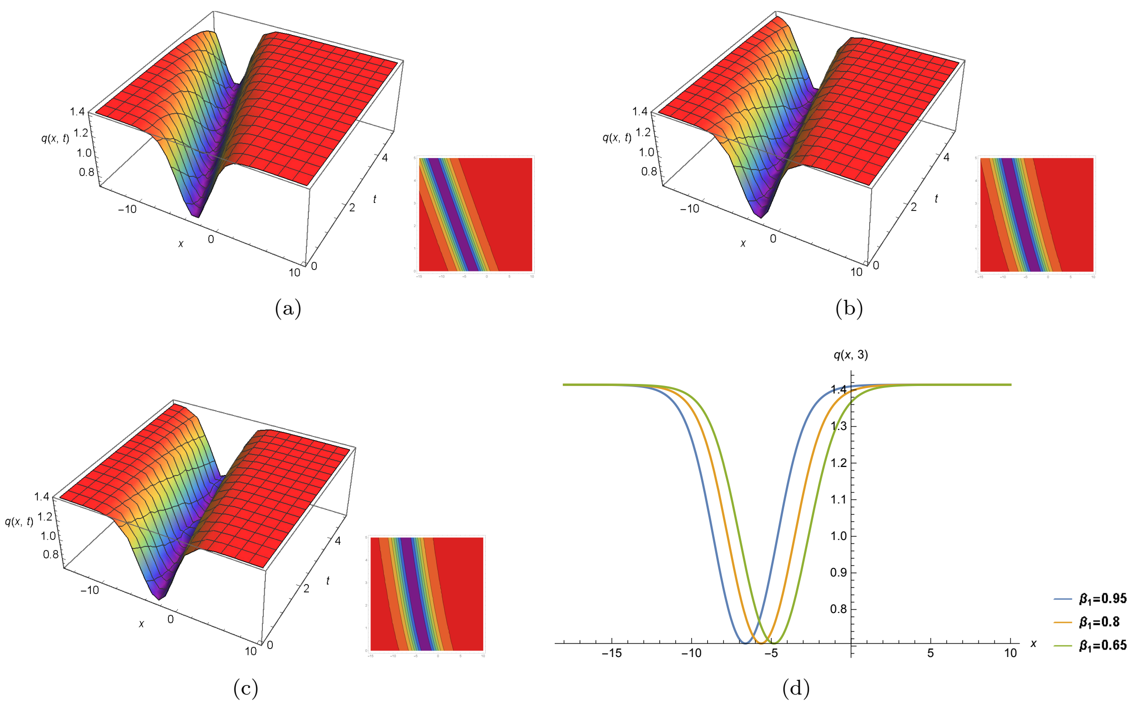


**Figure 15.** Graphical representations of the dark soliton solution given in (5.4) with parameters $\alpha = m = k = 1$, $a = -2$, $b = -3$, $c = -1$, $\lambda = 2$, $n = 3$, $\xi_0 = 0$ and $\beta_2 = 1$. (a)–(c) $3D$ and contour plots of the solution for $\beta_1 = 0.95$, 0.8, and 0.65, respectively, (d) $2D$ representations across various values of $\beta_1$.

- By applying the transformation (2.4) to Eq. (4.28), the following kink waves solution of Eq. (2.3) is obtained:

$$q(x,t) = \left(\frac{v_1}{2}\left[1 + \tanh\left(v_1\sqrt{\frac{-c}{3p}}\left(\lambda(t + \frac{1}{\Gamma(\beta_1)})^{\beta_1} + \alpha(x + \frac{1}{\Gamma(\beta_2)})^{\beta_2} - \xi_0\right)\right]\right)^{\frac{1}{2m}}. \quad (5.5)$$

The kink wave solutions arising from the variation of fractional orders $\beta_1$ in this solution are presented in Figure 16. The kink wave solutions arising from the variation of the fractional order $\beta_1$ in this solution are presented in Figure 16. Figures 16a–c show the 3D and contour representations of the kink wave profiles for different values of $\beta_1$, while Figure 16d illustrates the corresponding 2D wave profiles. It can be observed that decreasing $\beta_1$ causes the kink wave profile to shift rightward while preserving its overall wave structure.

The graphical results indicate that the beta fractional orders influence the wave behaviors of the obtained solutions in different ways. Depending on the type of wave structure, changes in the fractional orders may affect the oscillation period, wave position, or temporal behavior while preserving the main characteristics of the corresponding wave profiles.

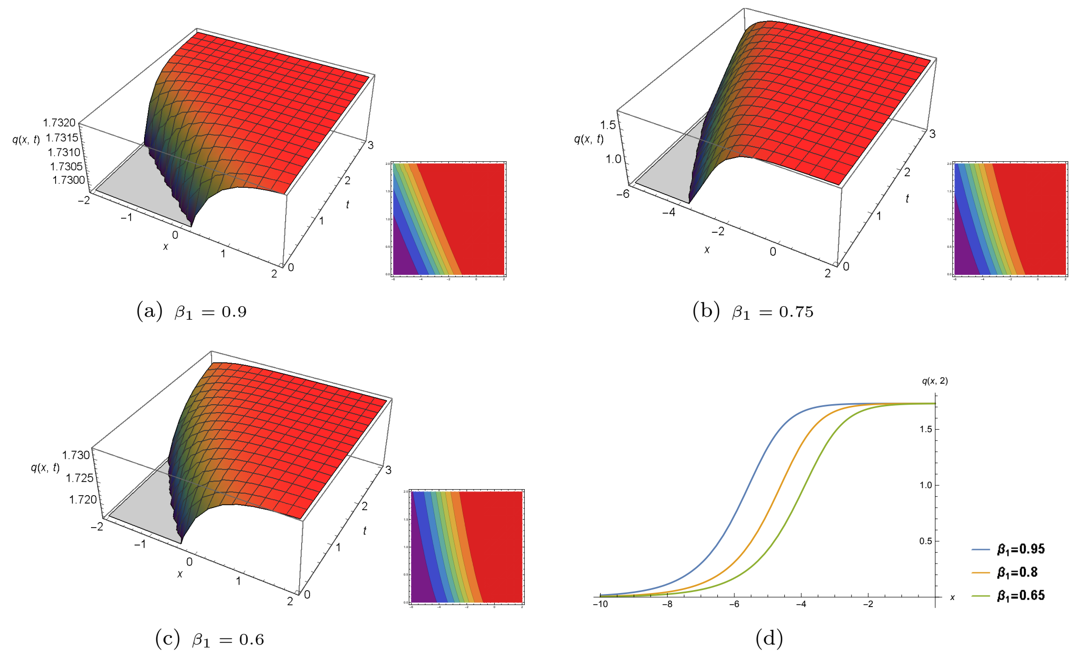


(a) $\beta_1 = 0.9$ (b) $\beta_1 = 0.75$

(c) $\beta_1 = 0.6$ (d)

**Figure 16.** Graphical representations of the kink wave solution given in (5.5) with parameters $\alpha = m = k = 1$, $a = -3$, $b = -4$, $c = -1$, $\lambda = 2$, $n = 3$, $\xi_0 = 0$ and $\beta_2 = 1$. (a)–(c) $3D$ and contour plots of the solution for $\beta_1 = 0.9$, 0.75, and 0.6, respectively, (d) $2D$ representations across various values of $\beta_1$.

# 6. Conclusion

This paper presents a rigorous investigation of the traveling wave solutions of the generalized Klein–Gordon equation with the beta fractional derivative via bifurcation analysis and planar dynamical systems techniques. Through an appropriate traveling wave transformation, the considered equation was reduced to a singular dynamical system containing singular point. Since the direct analysis of singular systems is generally difficult, a suitable time-scale transformation was introduced to convert the system into a regular dynamical system, which allowed the bifurcation and phase portrait analysis to be carried out effectively. A diverse set of traveling wave solutions, including periodic, singular periodic, dark and bright solitary, kink (or anti-kink), and some unbounded wave solutions, was obtained analytically. In addition, the stability and geometric behavior of the equilibrium points were explored through detailed phase portrait analysis, and sufficient parameter conditions for the existence of different types of traveling wave solutions in different regions of the parameter space were determined through the bifurcation structure.

The graphical representations further show that the fractional orders $\beta_1$ and $\beta_2$ influence different wave structures in different ways. For the singular periodic wave solutions, decreasing the fractional orders leads to temporal delay, longer oscillation periods, and broader spatial distributions. In the bright solitary, dark solitary, and kink-type wave solutions, the main wave structures are preserved, while the wave profiles exhibit noticeable spatial shifts for different values of the fractional orders.

The obtained results extend the study of generalized Klein–Gordon equations to the beta fractional derivative framework and provide further insight into the qualitative and dynamical properties of nonlinear wave solutions.

## Acknowledgements

We appreciate the reviewers' thorough review and helpful suggestions.

## References

[1] J. Ahmad and T. Younas, *Diverse optical wave structures to the time-fractional Phi-4 equation in nuclear physics through two powerful methods*, Opt. Quantum Electron., 2024, 56(4), 606.

[2] M. A. Almulhim and M. Al Nuwairan, *Bifurcation of traveling wave solution of Sakovich equation with beta fractional derivative*, Fractal Fract., 2023, 7(5), 372.

[3] M. Arab, *Bifurcation and exact traveling wave solutions for the nonlinear Klein-Gordon equation*, Eur. J. Pure Appl. Math., 2023, 16(4), 2643–2661.

[4] Asaduzzaman and M. A. Akbar, *Optical soliton solutions: The evolution with changing fractional-order derivative in Biswas–Arshed and Schrödinger Kerr law equations*, Opt. Quantum Electron., 2024, 56(3), 465.

[5] A. Atangana and B. S. T. Alkahtani, *Modeling the spread of Rubella disease using the concept of with local derivative with fractional parameter: Beta-derivative*, Complexity, 2016, 21(6), 442–451.

[6] A. Atangana, D. Baleanu and A. Alsaedi, *Analysis of time-fractional Hunter-Saxton equation: A model of neumatic liquid crystal*, Open Phys., 2016, 14(1), 145–149.

[7] A. Bekir, Ö. Güner and H. Bilgil, *Optical soliton solutions for the variable coefficient modified Kawahara equation*, Optik, 2015, 126(20), 2518–2522.

[8] M. Caputo and M. Fabrizio, *A new definition of fractional derivative without singular kernel*, Progr. Fract. Differ. Appl., 2015, 1(2), 73–85.

[9] Q. Chen, Y. Shang and H. Di, *Bifurcations and exact traveling wave solutions for the generalized nonlinear Schrödinger equation with wave operator*, J. Appl. Anal. Comput., 2022, 12(1), 336–346.

[10] Z. Cui, T. Lu and B. Chen, *Traveling wave solutions of the conformable fractional Klein–Gordon equation with power law nonlinearity*, J. Math., 2024, 2024(1), 8367957.

[11] Y. O. El-Dib, N. S. Elgazery and A. A. Mady, *Nonlinear dynamical analysis of a time-fractional Klein–Gordon equation*, Pramana – J. Phys., 2021, 95(4), 154.

[12] D. Feng, J. Li and J. Jiao, *Dynamical behavior of singular traveling waves of (n+1)-dimensional nonlinear Klein-Gordon equation*, Qual. Theory Dyn. Syst., 2019, 18(1), 265–287.

[13] D. Feng, J. Lü, J. Li and T. He, *Bifurcation studies on travelling wave solutions for nonlinear intensity Klein–Gordon equation*, Appl. Math. Comput., 2007, 189(1), 271–284.

[14] W. Hamali, A. A. Zaagan and H. Zogan, *Analysis of peakon-like soliton solutions: (3+1)-dimensional fractional Klein-Gordon equation*, AIMS Mathematics, 2024, 9(6), 14913–14931.

[15] M. D. Hossain, S. M. Boulaaras, A. M. Saeed, et al., *New investigation on soliton solutions of two nonlinear PDEs in mathematical physics with a dynamical property: Bifurcation analysis*, Open Phys., 2025, 23(1), 20250155.

[16] M. A. Islam, N. N. Rimu, S. Sarker, et al., *Dynamics of soliton solutions, bifurcation, chaotic behavior, stability, and sensitivity analysis of the time-fractional Gardner equation*, AIP Advances, 2025, 15(9).

[17] J. Jiang, Y. Gao, W. Zhang and L. Yin, *Bifurcation of traveling wave solutions of the $K(m,n)$ equation with generalized evolution term*, J. Appl. Anal. Comput., 2019, 9(3), 853–863.

[18] R. Khalil, M. Al Horani, A. Yousef and M. Sababheh, *A new definition of fractional derivative*, J. Comput. Appl. Math., 2014, 264, 65–70.

[19] J. Li, *Singular Nonlinear Travelling Wave Equations: Bifurcations and Exact Solutions*, Science Press, Beijing, 2013.

[20] J. Li and G. Chen, *On a class of singular nonlinear traveling wave equations*, Int. J. Bifurcation and Chaos, 2007, 17(11), 4049–4065.

[21] J. Li, Y. Zhang and G. Chen, *Exact solutions and their dynamics of traveling waves in three typical nonlinear wave equations*, Int. J. Bifurcation and Chaos, 2009, 19(07), 2249–2266.

[22] J. Li and Y. Zhou, *Bifurcations and exact traveling wave solutions for the nonlinear Schrödinger equation with fourth-order dispersion and dual power law nonlinearity*, Discrete Contin. Dyn. Syst. Ser. S, 2020, 13(11), 3083–3097.

[23] M. A. Mannaf, M. Jannah, M. H. Bashar, et al., *Exploring nonlinear dynamics and solitary waves in the fractional Klein–Gordon model*, Adv. Math. Phys., 2025, 2025(1), 9970003.

[24] M. Mirzazadeh, M. Eslami and A. Biswas, *Soliton solutions of the generalized Klein-Gordon equation by using $\left(\frac{G'}{G}\right)$-expansion method*, Comput. Appl. Math., 2014, 33, 831–839.

[25] I. Podlubny, *Geometric and physical interpretation of fractional integration and fractional differentiation*, Fract. Calc. Appl. Anal., 2002, 5(4), 367–386.

[26] A. R. Seadawy, A. Ali, A. Bekir, et al., *Novel exact solutions to the fractional PKP equation via mathematical methods*, Mod. Phys. Lett. A, 2025, 40(26), 2550099.

[27] M. Song, Z. Liu, E. Zerrad and A. Biswas, *Singular solitons and bifurcation analysis of quadratic nonlinear Klein-Gordon equation*, Appl. Math. Inf. Sci., 2013, 7(4), 1333.

[28] K. Wang, *New fractal soliton solutions for the coupled fractional Klein–Gordon equation with $\beta$-fractional derivative*, Fractals, 2023, 31(01), 2350003.

[29] I. Yalcinkaya, O. Tasbozan, A. Kurt and H. Ahmad, *Solution approximations for a mathematical model of relativistic electrons with beta derivative*, Appl. Math. J. Chinese Univ., 2024, 39(3), 469–485.

[30] C. Ye and W. Zhang, *New explicit solutions for the Klein–Gordon equation with cubic nonlinearity*, Appl. Math. Comput., 2010, 217(2), 716–724.

[31] M. Yu, C. Chen and Q. Zhang, *Bifurcations and exact solutions of the generalized Radhakrishnan–Kundu equation with the polynomial law*, Mathematics, 2023, 11(20), 4351.

[32] W. Yu, N. Li, F. Chen and S. Zhao, *Exact traveling wave solutions and bifurcations for the dullin-gottwald-holm equation*, J. Appl. Anal. Comput., 2016, 6(4), 968–980.

[33] L. Zhang, L.-Q. Chen and X. Huo, *The effects of horizontal singular straight line in a generalized nonlinear Klein–Gordon model equation*, Nonlinear Dyn., 2013, 72(4), 789–801.

[34] Y. Zhou and J. Li, *Bifurcations and exact solutions in the model of nonlinear elastodynamics of materials with strong ellipticity condition*, Nonlinear Dyn., 2024, 112(1), 1–13.

[35] W. Zhu, Y. Xia and Y. Bai, *Traveling wave solutions of the complex Ginzburg-Landau equation with kerr law nonlinearity*, Appl. Math. Comput., 2020, 382, 125342.

[36] J. Zhuang and Y. Zhou, *Bifurcations of solitary waves, periodic peakons and compactons of a coupled nonlinear wave equation*, J. Appl. Anal. Comput., 2022, 12(5), 1997–2013.

Received January 2026; Accepted July 2026; Available online July 2026.